



Frequency-Dependent Attenuation Characteristics of Coda and Body Waves in the Kumaun Himalaya: Implications for Regional Geology and Seismic Hazards

K. SIVARAM¹ and SANDEEP GUPTA¹

Abstract—We investigate the frequency-dependent seismic attenuation characteristics of the crust beneath Kumaun Himalaya, India, using seismic coda waves (Q_c^{-1}) and high-frequency body waves (Q_x^{-1} and Q_β^{-1}). We used about 300 local earthquakes, well-recorded by 32 three-component broadband stations, for characterizing the seismic attenuation. The corresponding geodynamic implications are analyzed for the entire study region and for major tectonic segments such as the Lesser Himalaya (LH) and the Higher Himalaya (HH). The coda quality factor, Q_c , computed from the single backscattering model, shows a dependence on both frequency (1–20 Hz) and lapse times (20–50 s). Expressed as power laws ($Q_c = Q_0 f^n$), Q_0 (Q at 1 Hz) and n (frequency-dependence exponent) vary as 320 and 0.78 for lapse time window (LTW) 20 s to 656 and 0.55 at LTW 50 s. Similarly, the Q factor of body waves (Q_x and Q_β), computed using the coda normalization and extended coda normalization methods (Yoshimoto et al. Geophys J Int 114: 165–174, 1993), also show strong frequency dependence. They are expressed as $Q_x = (36.28 \pm 0.05)f^{(0.85 \pm 0.01)}$ and $Q_\beta = (50.58 \pm 0.15)f^{(0.94 \pm 0.01)}$. The ratio Q_β/Q_x is found to be larger than unity in the whole frequency range for the entire study region. This observation is interpreted as an effect from seismically active regions and heterogeneous crustal regimes. Additionally, to characterize the dominant attenuation mechanism, we separate the quality factors for intrinsic attenuation (Q_i^{-1}) and scattering attenuation (Q_s^{-1}), using the Wennerberg (Bull Seismol Soc Am 83:279–290, 1993) formulation. Our study shows that the seismic attenuations are different for the LH and the HH segments. This possibly is due to the mechanism of underthrusting and deformation in the LH segments, leading to a dominant scattering attenuation and the multitude of fractures and pores in the crust. Our study shows that (1) Q_c^{-1} is less than Q_β^{-1} , which seems to adhere to Zeng's (J Geophys Res 96:607–619, 1991) theory; (2) Q_c^{-1} is closer to Q_i^{-1} ; (3) the ratio (Q_x^{-1}/Q_β^{-1}) lies between 1.7 and 2.25. The results are in agreement with several theoretical and laboratory experiments and suggest heterogeneous crustal media. The varying attenuation characteristics, seismic energy budget and radiating efficiency have a significant role in seismic hazard analysis in Kumaun Himalaya.

Keywords: Seismic coda waves, body waves, attenuation, Kumaun Himalaya.

1. Introduction

The Himalayan orogeny has resulted from multiple factors, summarized as large-scale interactions between lithospheric deformation and atmospheric circulations. The Indian-Eurasian plate collision processes have yielded a diversity of geological features such as large-scale thrust, strike-slip and normal fault systems, which are exhaustively described in geological studies (Bilham et al., 1997; Burg & Chen, 1984; Burchfiel et al., 1992; Larson et al., 1999; Tapponnier et al., 1986) and regional metamorphism (Le Fort, 1996; Searle, 1991). The Himalayan orogen is supposed to have played a critical role in controlling climate change (Molnar et al., 1993). Among the most significant magmatic products resulting from the Indian-Eurasian plate collision are the High Himalayan leucogranites (HHL) formed around 25–18 Ma at about 400 MPa pressure, corresponding to a depth of 8–15 km (Le Fort et al., 1987). The present challenge is to understand the seismic attenuation beneath different seismotectonic segments augmenting the knowledge of the seismic energy budget in the study region. The Kumaun Himalaya is our study region, which is a complex seismo-tectonically active region, emplaced with major tectonic features like the Southern Tibetan Detachment (STD), Main Central Thrust (MCT), Main Boundary Thrust (MBT) and Main Frontal Thrust (MFT). Diverse models have tried to explain the evolution, tectonics and seismicity, e.g., the steady-state model (Seeber & Armbruster, 1981) and evolutionary model (Ni & Barazangi, 1984). The cause for the occurrence of small and large earthquakes is the high-strain accumulation due to Indo-Eurasian plate collision along different Himalayan

¹ CSIR-National Geophysical Research Institute, Uppal Road, Hyderabad 500007, India. E-mail: sivaramk@ngri.res.in

frontal thrusts, within different tectonic belts such as the Lesser Himalaya (LH) and the Higher Himalaya (HH) segments. From the perspective of seismic hazard analysis, a regional seismic model is needed which facilitates quicker estimation of the ground motion intensity measures and describes the energy-attenuation process from the source region to the measurement region. This fundamentally also facilitates the knowledge of the rock properties through which the seismic waves propagate with the aid of the various measures of Q (quality factor, inverse of attenuation) (Knopoff, 1964), such as Q_c (coda Q); Q_β and Q_α (S-wave and P-wave Q) (or body wave Q). In general, the total attenuation (or Q^{-1}) is a combination of intrinsic and scattering attenuation (Aki, 1969, 1980; Aki & Chouet, 1975). According to laboratory experiments, Vassiliou et al. (1982) have provided valuable relations between Q_β and Q_α for different conditions of rock, such as: $Q_\beta = Q_\alpha$ for dry rocks, $Q_\beta \geq Q_\alpha$ for partially saturated rocks and $Q_\beta \leq Q_\alpha$ for fully saturated rocks. Winkler and Nur (1982) have provided additional relations between $\left(\frac{Q_\beta}{Q_\alpha}\right)$ and $\left(\frac{V_\alpha}{V_\beta}\right)$ (V_α = velocity of P waves, V_β = velocity of S waves) in characterizing the petrological properties of the upper crust. Several researchers correlate the variations of the various diagnostic parameters and frequency-dependent estimates of Q with the geology and seismotectonics of the study area (Giampiccolo et al., 2002; Jin & Aki, 1989; Matsumoto & Hasegawa, 1989; Ma & Huang, 2020; Patane et al., 1994, 2011; Rautian & Khalturin, 1978; Sato, 1982; Sharma et al., 2008; Singh & Herrmann, 1983; Tripathi et al., 2014; Yoshimoto et al., 1993).

In the Himalayas, some of the seismic attenuation (Q^{-1}) studies in several smaller regions include Mukhopadhyay et al. (2006) in the northwestern Himalaya region, Mukhopadhyay and Sharma (2010), Mukhopadhyay et al. (2010) in Garhwal-Kumaun Himalaya, Ashish et al. (2009), Singh et al. (2012) in the Kumaun Himalaya, Tripathi et al. (2014) in Garhwal Himalaya, Mishra et al. (2020) in northwestern Himalaya and Monika et al. (2020) in Garhwal and Kumaon Himalaya. Due to the different techniques, constraints on the dataset and sampling regions, some of these studies show slightly varying results. Among the larger data set studies,

Mukhopadhyay et al. (2010) investigate the seismic attenuation (Q^{-1} factors) using the Multiple Lapse Time Window Analysis (MLTWA) technique. In a region similar to ours, Monika et al. (2020) explores the body-wave Q^{-1} factors using similar methods as we used. Seismic tomography studies attempted in this region (Gupta et al., 2022; Mahesh et al., 2012) using local earthquakes relate their observed anomalous velocity variations with the possible partial melts and diverse metamorphism. Similarly, Sheehan et al. (2014) observed a zone characterized by high body wave attenuation and low $\left(\frac{V_\alpha}{V_\beta}\right)$ beneath the Lesser Himalaya in Nepal.

An unresolved issue in Kumaun Himalaya is the relative contributions of the Q_i (quality factor corresponding to intrinsic attenuation) and Q_s (quality factor corresponding to the scattering attenuation), which enhance the knowledge of crustal properties beneath Kumaun Himalaya. Scattering attenuation (Q_s^{-1}) signifies the heterogeneity of the rocks in the crust that rearranges the seismic energy without loss whereas Q_i^{-1} characterizes the intrinsic anelasticity that changes the seismic energy into frictional heat, mostly along grain boundaries, and is closely associated with high temperature or heat flow. Thus, we envisage providing a detailed attenuation study (based on various estimates of Q^{-1} from various phases of the seismograms) for Kumaun Himalaya, thereby enabling the analysis of crustal rock structure for seismic hazard assessment, which will act as highly valuable inferences for both the seismologists and engineers. The single scattering model (Aki & Chouet, 1975) has been used to calculate Q_c values, the coda normalization (CN) (Aki, 1980) and the extended coda normalization (ECN) methods (Yoshimoto et al., 1993) to obtain body wave Q values in the frequency range 1 to 20 Hz.

2. Seismotectonic Setting and Broadband Data Acquisition

The study region is Kumaun Himalayan region (latitude 29°N–31°N, longitude 78°E–81°E), which forms a part of the Himalayas, resulting from the underthrusting of the Indian plate with the Eurasian

continental plate, after the closure of the Tethys Ocean and a following long geological evolution. The surface expression of major tectonic features of the region comprises the STD, MCT, MBT and MFT. The LH segment is structurally bounded by the MBT and MCT zone and consists of predominantly Pre-cambrian clastic sediments. The HH segment is bounded by the lower limit of MCT zone and STD, comprising early Cambrian metasedimentary rocks. The data set consists of the broadband seismograms recorded during June 2005–June 2008 in a seismograph network operated by CSIR National Geophysical Research Institute. Figure 1 shows the seismic network along with the major tectonic features (see also Mahesh et al., 2013). Table 1 shows the details of stations considered in this study, which are segregated as per the LH and HH segments. The broadband stations are installed with Guralp CMG-3 T triaxial broadband seismometer (having a flat velocity response in 0.0083-Hz (120-s period) to 50-Hz frequency range). They are attached to 24-bit (Reftek/Trimble make) RT-130/1 digital data acquisition system and synchronized by global positioning

system (GPS). The broadband stations were located on rock or stiff soil profiles and also observed to have minimum noise interference. The data were recorded at a sampling rate of 50 samples/s, and periodic maintenance was undertaken to ensure that all the stations were synchronized and operating in continuous mode.

3. Methodology and Data Analysis

In this study, about 300 local earthquakes and corresponding digital broadband seismograms recorded at 32 seismic stations across Kumaun Himalaya were selected based on good S/N (signal to noise ratio, $S/N > 2$) and clear P-wave and S-wave arrivals. The magnitude of the selected local events is < 5 and focal depths < 25 km (for details, see Mahesh et al., 2012, 2013). The seismograms were Butterworth bandpass (4 pole) filtered at five central frequencies: 1.5 (1–3 Hz), 3 (2–4 Hz), 6 (4–8 Hz), 8 (6–10 Hz), 12 (8–16 Hz) and 18 (12–24 Hz). The P-wave

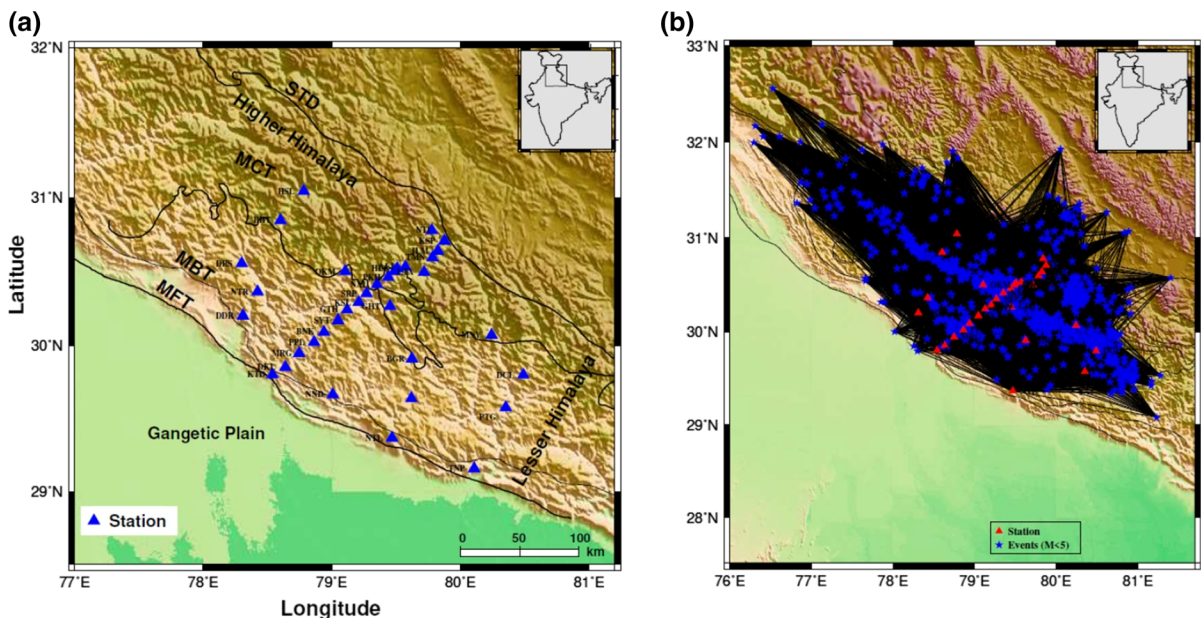


Figure 1

a Tectonic map of Kumaun Himalaya shown with 32 broadband seismic stations (blue triangles). *MFT* Main Frontal Thrust, *MBT* Main Boundary Thrust, *MCT* Main Central Thrust, *STD* Southern Tibet Detachment. **b** The sampled study region showing the ray paths of local earthquakes (blue stars) and recording stations (red triangles) used in the estimation of seismic attenuation

Table 1

Details of the broadband recording stations used in this study for investigating seismic attenuation, which are segregated under the Lesser Himalaya (LH) and the Higher Himalaya (HH) segments

Lesser Himalaya				Higher Himalaya			
S.no.	Station	Lat (°N)	Long (°E)	S.no.	Station	Lat (°N)	Long (°E)
1	ALM	29.64	79.62	1	BHT	30.85	78.60
2	DKL	29.86	78.64	2	GHT	30.26	79.45
3	BGR	29.91	79.62	3	HLG	30.52	79.51
4	BNK	30.09	78.94	4	LGS	30.50	79.49
5	DCL	29.80	80.49	5	MNY	30.07	80.24
6	DDR	30.20	78.31	6	NAL	30.41	79.35
7	DRS	30.55	78.30	7	OKM	30.50	79.10
8	GTH	30.24	79.12	8	PKH	30.46	79.44
9	KSL	30.29	79.21	9	ALI	30.53	79.57
10	KTD	29.80	78.54	10	HSL	31.04	78.78
11	MRG	29.95	78.75	11	JLM	30.64	79.83
12	NND	29.67	79.01	12	KSP	30.71	79.88
13	NTL	29.37	79.47	13	LTA	30.50	79.72
14	NTR	30.36	78.42	14	NTI	30.78	79.84
15	PPL	30.02	78.86				
16	PTG	29.58	80.35				
17	SRP	30.35	79.27				
18	SYT	30.17	79.05				

analysis is based on vertical (Z) component seismograms, and the S-wave analysis is based on E-W (east-west) and N-S (north-south) component seismograms. Figure 2 shows the sample data processing steps and bandpass filtering on a raw seismogram for station GTH.

In the first part, Q_c values are estimated, assuming the single backscattering model proposed by Aki and Chouet (1975). In this model, the outgoing body waves are scattered only once before reaching the recording station. The coda waves as seen in the decreasing tail portion of a seismogram, are interpreted as backscattered body waves generated by multiple small-scale heterogeneities existing in the crust and upper mantle. Using the Aki (1980) model, the coda amplitude in a seismogram, as a function of central frequency, f , in a certain narrow bandwidth, and the lapse time, t , which is measured from the origin time of the earthquake, can be expressed as:

$$A_c(f, t) = S(f)t^{-\gamma}e^{-\frac{\pi ft}{Q_c}}, \quad (1)$$

where $S(f)$ is the source function at frequency f . Here, factor γ is the geometrical spreading factor, and Q_c is

the apparent quality factor of the coda waves associated with the attenuation in the medium. Considering $\gamma = 1$, representative of scattered body waves, the above Eq. (1) can be re-written as

$$\ln[A_c(f, t)t] = \ln S(f) - \left(\frac{\pi f}{Q_c}\right)t \quad (2)$$

The above linear Eq. (2) has a slope $-\pi f/Q_c$, from which Q_c can be estimated.

The coda spectral amplitude, $A_c(f, t_c)$, is derived from the root mean square (r.m.s) amplitude for the time window of 5 s for different lapse times. A sliding time window (or moving average) of size 250 data samples (corresponding to 5 s) is used and then advanced through the window lengths from 20 to 50 s corresponding to different lapse times. Figures 2 and 3 show the example steps in data processing for Q_c estimation for the seismic station GTH.

In the second part, the coda normalization (CN) method introduced by Aki (1980) and modified as extended coda normalization (ECN) method, by Yoshimoto et al. (1993) is used to compute Q_β , Q_α . The CN method is suggested as a single-station method to normalize the spectral amplitude of the earthquake source by that of the coda waves at fixed lapse time, which is done here by comparing S wave (or P wave) and coda wave amplitudes of events at different hypocentral distances, followed by the division of the amplitude of direct S-wave by the coda amplitude measured at fixed lapse times t_c .

The spectral amplitude of the direct S wave, $A_s(f, r)$, is expressed as

$$A_s(f, r) = R_{\theta\phi}I(f)S_s(f)G(f)r^{-\gamma}e^{\left[\frac{-\pi fr}{Q_\beta(f)V_\beta}\right]}, \quad (3)$$

where $R_{\theta\phi}$ is the source radiation pattern, γ is the geometrical spreading exponent, $Q_\beta(f)$ is the S wave quality factor, and V_β is the average S wave velocity.

For lapse times greater than roughly twice the direct S-wave travel time, and considering the effects of factors like the coda excitation factor $P(f, t_c)$, source spectral amplitude of S waves $S_s(f)$, site effect $G(f)$ and the recording instrumental response $I(f)$, the spectral amplitude of the coda wave is expressed as

$$A_c(f, t_c) = S_s(f)P(f, t_c)G(f)I(f). \quad (4)$$

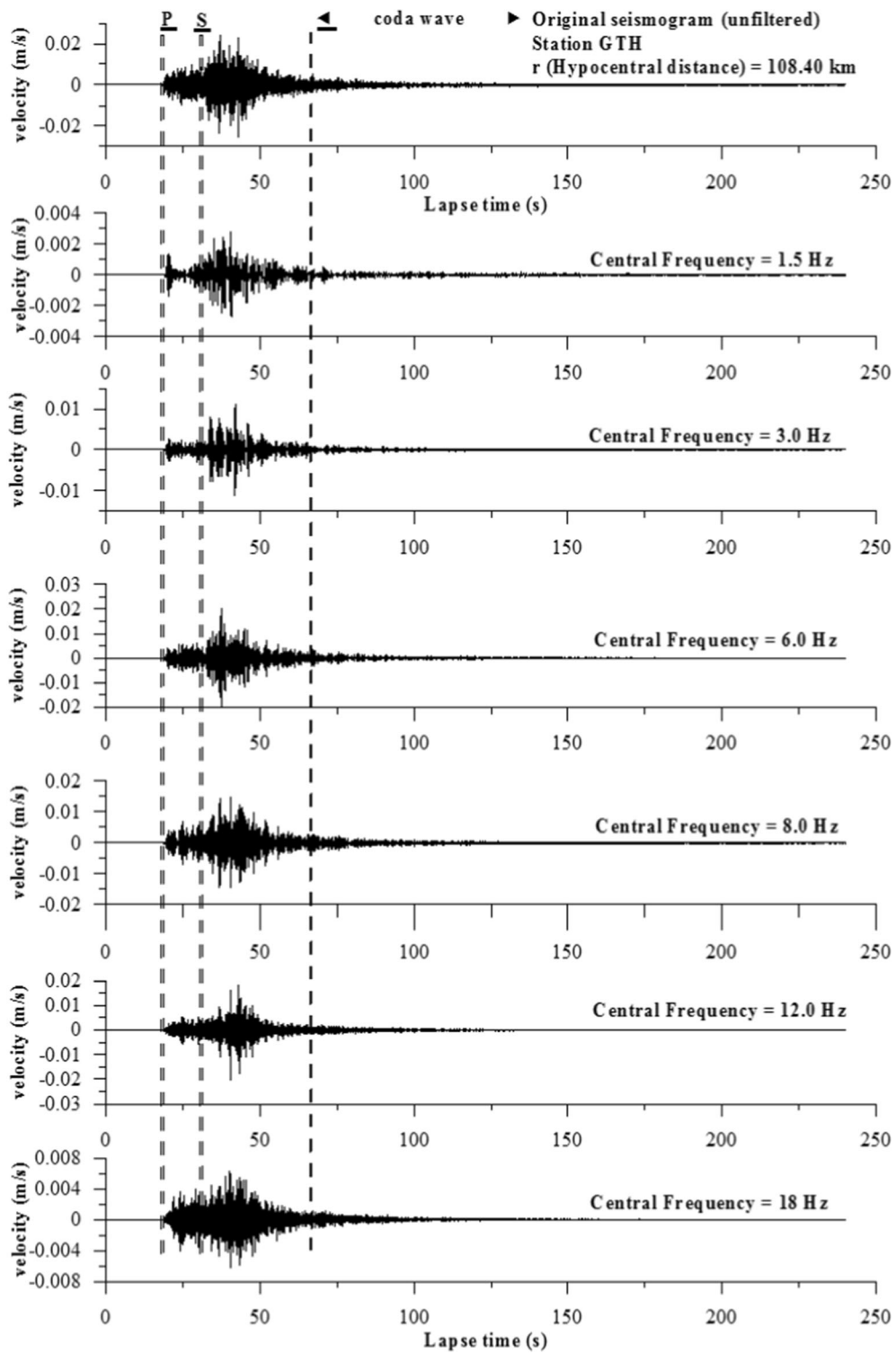


Figure 2

Original and filtered seismograms of an event recorded at GTH (Gaithi) seismic station for six central frequencies (C.F.) (1.5, 3, 6, 8, 12 and 18 Hz)

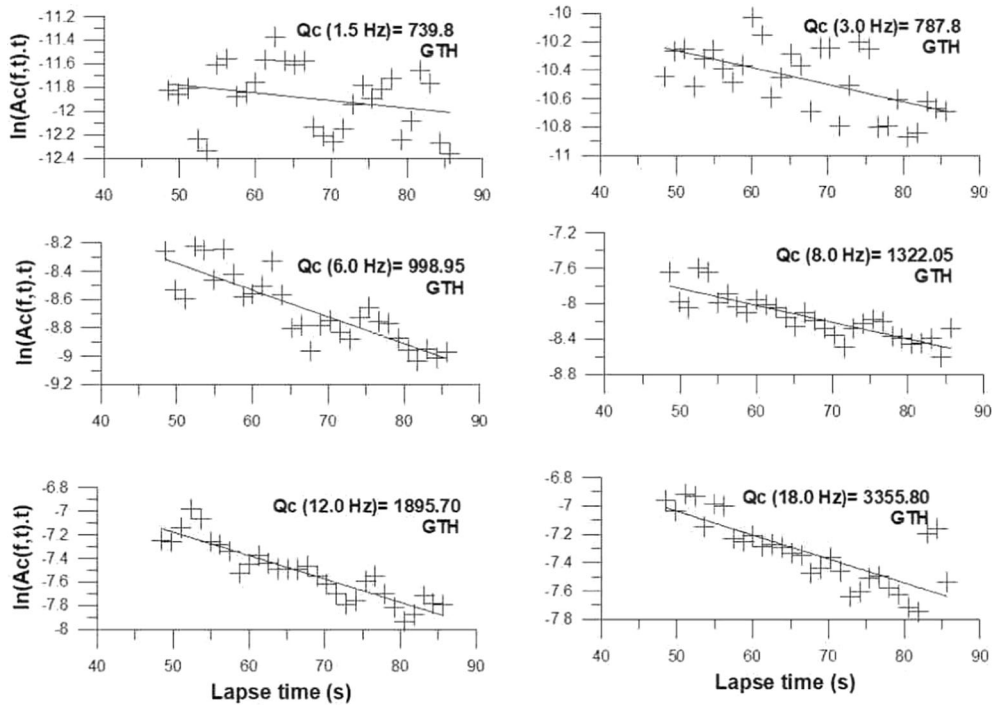


Figure 3
Variation of $\ln[A_c(f, t)t]$ with lapse time t at the six central frequencies for the seismograms as shown in Fig. 2

After dividing Eq. (3) by Eq. (4), and taking the natural logarithm, we get the equation for attenuation of the direct S waves as

$$\left[\ln \left(\frac{A_s(f, r)r^\gamma}{A_c(f, t_c)} \right) \right] = \frac{-\pi f}{Q_\beta(f)V_\beta} r + \text{constant}(f). \quad (5)$$

In the above Eq. (5), division by the coda amplitudes is presumed to remove the site effects so that amplitudes from different stations can be compared. Another assumption is that averaging over a number of S waves from events at different azimuths diminishes the effect of the radiation pattern, $R_{\theta\phi}$. Here, Q_β can be computed from the linear regression of $\left[\ln \left(\frac{A_s(f, r)r^\gamma}{A_c(f, t_c)} \right) \right]$ versus hypocentral distance and r by means of least squares method.

The same methodology as used in the CN method is extended to P-wave ECN method as proposed by Yoshimoto et al. (1993) for direct P wave. The ECN method stands on the assumption that earthquakes within a small magnitude range (in this study, $M < 5$) have the same spectral ratio of P to S wave radiation within a narrow frequency range and existence of a

proportionality among the coda spectral amplitude, A_c , the source spectral amplitude of S waves, S_s , and the source spectral amplitude of P waves, S_p , as follows:

$$A_c(f, t_c) \propto S_s(f) \propto S_p(f), \quad (6)$$

which implies that we can use the spectral amplitude of the S-wave coda for the normalization of P-wave spectral amplitude. Using Yoshimoto et al. (1993), a similar equation for P waves is expressed as

$$\left[\ln \left(\frac{A_p(f, r)r^\gamma}{A_c(f, t_c)} \right) \right] = \frac{-\pi f}{Q_\alpha(f)V_\alpha} r + \text{constant}(f), \quad (7)$$

where V_α is the average P wave velocity. Q_α (for P waves) is obtained from the linear least squares regression of $\left[\ln \left(\frac{A_p(f, r)r^\gamma}{A_c(f, t_c)} \right) \right]$ versus hypocentral distance, r .

It is also observed that the CN and ECN methods are effective techniques for combining amplitudes from different earthquakes and stations of a sub-region on the same plot to assess the average attenuation characteristics of that sub-region by

Table 2

Estimated values of the coda quality factors Q (at 1 Hz) and exponent of frequency dependence 'n' along with corresponding ± 1 standard deviation (1σ) for different lapse time windows (LTWs)

S.no.	Station	LTW = 20 s	LTW = 30 s	LTW = 40 s	LTW = 50 s
$Q_0 \pm 1\sigma$					
1	ALM	206 \pm 10	265 \pm 9	531 \pm 7	834 \pm 5
2	DKL	93 \pm 7	319 \pm 3	471 \pm 17	564 \pm 8
3	BGR	84 \pm 2	194 \pm 2	468 \pm 8	428 \pm 13
4	BNK	276 \pm 7	252 \pm 5	316 \pm 3	399 \pm 4
5	DCL	128 \pm 1	81 \pm 0.5	112 \pm 4	116 \pm 1
6	DDR	120 \pm 54	477 \pm 7	236 \pm 1	306 \pm 1
7	DRS	182 \pm 7	219 \pm 3	299 \pm 10	231 \pm 2
8	GTH	226 \pm 2	256 \pm 5	397 \pm 9	299 \pm 3
9	KSL	101 \pm 7	159 \pm 1	177 \pm 2	338 \pm 7
10	KTD	105 \pm 1	150 \pm 2	146 \pm 6	242 \pm 6
11	MRG	104 \pm 1	167 \pm 1	349 \pm 5	383 \pm 9
12	NND	144 \pm 2	237 \pm 14	193 \pm 1	357 \pm 2
13	NTL	128 \pm 3	109 \pm 5	279 \pm 3	324 \pm 21
14	NTR	153 \pm 4	229 \pm 1	423 \pm 7	401 \pm 20
15	PPL	117 \pm 6	151 \pm 1	193 \pm 1	313 \pm 4
16	PTG	179 \pm 14	156 \pm 2	244 \pm 2	530 \pm 7
17	SRP	108 \pm 6	128 \pm 3	309 \pm 6	265 \pm 5
18	SYT	112 \pm 1	180 \pm 2	174 \pm 5	258 \pm 3
19	BHT	141 \pm 1	120 \pm 6	144 \pm 2	216 \pm 1
20	GHT	108 \pm 4	203 \pm 4	214 \pm 3	232 \pm 3
21	HLG	148 \pm 6	144 \pm 1	143 \pm 1	170 \pm 1
22	LGS	112 \pm 8	83 \pm 3	190 \pm 9	228 \pm 2
23	MNY	94 \pm 2	122 \pm 2	120 \pm 1	133 \pm 1
24	NAL	166 \pm 1	202 \pm 1	183 \pm 1	305 \pm 4
25	OKM	74 \pm 1	174 \pm 2	169 \pm 6	198 \pm 8
26	PKH	124 \pm 4	132 \pm 1	222 \pm 3	218 \pm 4
27	ALI	87 \pm 8	105 \pm 2	115 \pm 1	122 \pm 9
28	HSL	91 \pm 5	282 \pm 8	315 \pm 4	217 \pm 3
29	JLM	27 \pm 1	42 \pm 4	157 \pm 5	168 \pm 9
30	KSP	100 \pm 5	98 \pm 1	281 \pm 9	217 \pm 4
31	LTA	32 \pm 10	157 \pm 9	180 \pm 24	304 \pm 6
32	NTI	108 \pm 28	132 \pm 3	152 \pm 1	184 \pm 1
Average		122 \pm 7	176 \pm 3	238 \pm 5	280 \pm 6
$n \pm 1\sigma$					
1	ALM	0.89 \pm 0.05	1.01 \pm 0.04	0.70 \pm 0.03	0.53 \pm 0.02
2	DKL	1.48 \pm 0.04	0.74 \pm 0.01	0.55 \pm 0.02	0.51 \pm 0.01
3	BGR	1.23 \pm 0.01	0.89 \pm 0.01	0.53 \pm 0.01	0.63 \pm 0.01
4	BNK	1.46 \pm 0.01	0.77 \pm 0.02	0.66 \pm 0.01	0.57 \pm 0.01
5	DCL	1.06 \pm 0.01	1.23 \pm 0.01	1.13 \pm 0.02	1.15 \pm 0.01
6	DDR	2.02 \pm 0.02	0.64 \pm 0.01	0.88 \pm 0.01	0.78 \pm 0.01
7	DRS	0.96 \pm 0.02	0.93 \pm 0.08	0.83 \pm 0.02	0.92 \pm 0.01
8	GTH	0.92 \pm 0.01	0.84 \pm 0.01	0.58 \pm 0.01	0.73 \pm 0.01
9	KSL	1.28 \pm 0.04	1.05 \pm 0.04	1.00 \pm 0.05	0.75 \pm 0.01
10	KTD	1.24 \pm 0.04	1.17 \pm 0.01	1.21 \pm 0.03	1.02 \pm 0.01
11	MRG	1.21 \pm 0.01	0.93 \pm 0.01	0.63 \pm 0.01	0.64 \pm 0.01
12	NND	0.97 \pm 0.01	0.92 \pm 0.04	0.95 \pm 0.04	0.76 \pm 0.03
13	NTL	1.02 \pm 0.01	1.40 \pm 0.03	0.98 \pm 0.01	1.05 \pm 0.04
14	NTR	1.11 \pm 0.01	0.86 \pm 0.02	0.63 \pm 0.01	0.71 \pm 0.03
15	PPL	1.18 \pm 0.03	0.94 \pm 0.05	0.85 \pm 0.04	0.68 \pm 0.06
16	PTG	0.91 \pm 0.05	0.82 \pm 0.01	0.69 \pm 0.01	0.49 \pm 0.02
17	SRP	1.34 \pm 0.03	1.17 \pm 0.01	0.73 \pm 0.01	0.81 \pm 0.01
18	SYT	1.14 \pm 0.01	0.93 \pm 0.01	0.98 \pm 0.02	0.82 \pm 0.01
19	BHT	1.08 \pm 0.01	1.23 \pm 0.03	1.03 \pm 0.06	0.94 \pm 0.01

Table 2 *continued*

S.no.	Station	LTW = 20 s	LTW = 30 s	LTW = 40 s	LTW = 50 s
20	GHT	0.95 ± 0.01	0.93 ± 0.01	0.92 ± 0.01	0.97 ± 0.01
21	HLG	1.11 ± 0.01	1.10 ± 0.02	1.03 ± 0.03	1.15 ± 0.01
22	LGS	1.27 ± 0.04	1.34 ± 0.02	1.10 ± 0.02	0.98 ± 0.01
23	MNY	1.13 ± 0.01	1.10 ± 0.01	1.12 ± 0.03	1.14 ± 0.01
24	NAL	1.02 ± 0.01	0.93 ± 0.01	0.98 ± 0.01	0.93 ± 0.01
25	OKM	1.39 ± 0.01	0.98 ± 0.01	0.97 ± 0.02	1.01 ± 0.02
26	PKH	1.08 ± 0.01	1.06 ± 0.01	0.87 ± 0.01	1.02 ± 0.01
27	ALI	1.65 ± 0.05	1.36 ± 0.01	1.37 ± 0.01	1.50 ± 0.04
28	HSL	1.30 ± 0.03	0.74 ± 0.02	0.72 ± 0.01	1.01 ± 0.01
29	JLM	1.20 ± 0.02	0.69 ± 0.05	1.09 ± 0.02	0.36 ± 0.01
20	KSP	1.00 ± 0.02	1.12 ± 0.01	0.75 ± 0.02	0.91 ± 0.01
31	LTA	1.08 ± 0.11	1.06 ± 0.03	0.95 ± 0.04	0.94 ± 0.01
32	NTI	1.2 ± 0.05	1.14 ± 0.02	1.05 ± 0.01	0.98 ± 0.01
Average		1.19 ± 0.02	1.00 ± 0.02	0.90 ± 0.02	0.86 ± 0.02

estimating the Q_β and Q_s , respectively, from slopes using Eqs. (5) and (7). In this paper, we report direct body wave Q values determined after fixing the geometrical spreading as r^{-1} (with $\gamma = 1$) and letting Q vary with frequency so that these estimates can be comparable to other studies that use frequency-dependent Q estimates.

The scatterers accountable for the generation of coda waves are largely assumed to be distributed over the surface area of an ellipsoid (Pulli, 1984; Sato, 1978) and can be computed from relations such as

$$\frac{X^2}{\left(\frac{vt}{2}\right)^2} + \frac{Y^2}{\left(\frac{vt}{2} - r\right)^2} = 1, \tag{8}$$

where X and Y denote the major and minor axes of the ellipsoid; r is the distance between the earthquake source and the recording station; v and t represent the velocity of S wave (3.4 km/s; Mahesh et al., 2013) and lapse time (40 s), respectively. As per Aki and Chouet (1975), if r equals zero, then the Eq. (8) represents the circular area of radius $vt/2$, i.e., 68 km and a circular area (of scatterers) of 14,519 km².

The third part of the computation consists of the extraction of the quality factors corresponding to intrinsic and scattering attenuation, namely, Q_i and Q_s . In recent years, several researchers have attempted to separate the contribution of intrinsic and scattering attenuation. According to Zeng et al. (1991) and Wennerberg (1993), Q_i and Q_s can be estimated from Q_c and Q_β as

$$Q_c^{-1} = Q_i^{-1} + \frac{\{1 - 2\delta(\tau)\}}{Q_s}, \tag{9}$$

where

$$\delta(\tau) = \frac{0.72}{(4.44 + 0.738\tau)} - 0.5, \tag{10}$$

$$\tau = \frac{\omega t}{Q_s}, \tag{11}$$

and ω and t are the angular frequency and the lapse time respectively.

If Q_d describes the total quality factor for direct S waves, it can be expressed as the sum of inverse of intrinsic and scattering attenuation, as

$$\frac{1}{Q_d} = \frac{1}{Q_i} + \frac{1}{Q_s}. \tag{12}$$

From which Q_s and Q_i are derived as follows (Wennerberg, 1993):

$$\frac{1}{Q_s} = \left\{ \frac{1}{2\delta(\tau)} \right\} \left\{ \frac{1}{Q_d} - \frac{1}{Q_c(\tau)} \right\}, \tag{13}$$

$$\frac{1}{Q_i} = \left\{ \frac{1}{2\delta(\tau)} \right\} \left\{ \frac{1}{Q_c(\tau)} + \frac{[2\delta(\tau) - 1]}{Q_d} \right\}. \tag{14}$$

Considering Eqs. (8) to (14), Q_s is obtained from the positive root of the quadratic equation:

Table 3

Estimated values of the quality factors Q_c for each lapse time window (LTW) and at six central frequencies (CFs). The frequency-dependent $Q_c(f)$ for the entire region is also shown

CF	Q_c
LTW 20 s	
1.5	418.41
3	783.44
6	1394.96
8	1664.47
12	2087.58
18	3080.47
Whole region $Q_c(f) = Q_0 f^n$	
	$(319.99 \pm 0.45)f^{(0.78 \pm 0.01)}$
CF	Q_c
LTW 30 s	
1.5	480.47
3	1108.24
6	1481.07
8	1643.48
12	2245.08
18	3074.04
Whole region $Q_c(f) = Q_0 f^n$	
	$(417.91 \pm 3.12)f^{(0.69 \pm 0.01)}$
CF	Q_c
LTW 40 s	
1.5	742.95
3	1163.40
6	1466.36
8	1802.65
12	2386.84
18	3485.40
Whole region $Q_c(f) = Q_0 f^n$	
	$(470.16 \pm 2.05)f^{(0.59 \pm 0.01)}$
CF	Q_c
LTW 50 s	
1.5	810.53
3	1421.08
6	1509.87
8	1786.29
12	2680.37
18	3574.25
Whole region $Q_c(f) = Q_0 f^n$	
	$(656.40 \pm 5.67)f^{(0.55 \pm 0.01)}$

$$4.44 \left(\frac{1}{Q_d} - \frac{1}{Q_c} \right) Q_s^2 + \left[0.738 \left(\frac{1}{Q_d} - \frac{1}{Q_c} \right) \omega t - 5.88 \right] Q_s - 0.738 \omega t = 0, \quad (15)$$

and Q_i is similarly obtained from the positive value of Q_s as:

$$Q_i = Q_d \left(\frac{Q_s}{Q_s - Q_d} \right). \quad (16)$$

The root mean square (rms) amplitudes of the coda waves were determined for each waveform in each frequency band, with the window lengths at 5 s. Figures 2 and 3 show the example steps in data processing for Q_c estimation for the seismic station GTH.

4. Results and Discussion

The computations and the corresponding seismic attenuation models are separately shown below for Q_c , Q_β , Q_α , Q_i and Q_s .

4.1. Seismic Attenuation Model from Q_c

As shown in Figs. 2 and 3, the outline of the estimation of Q_c is depicted for the representative seismic station GTH. The average Q_c values were obtained after averaging all the individual Q_c values. The estimates of Q_0 and n along with 1σ (standard deviation) for different stations and different lapse times are shown in Table 2. In Table 3, we show the estimated values of the quality factors Q_c for each lapse time window (LTW) and at different (six) central frequencies (CFs). The frequency-dependent $Q_c(f)$ for the entire region is also shown.

Figure 4 shows the variation of Q_0 (Q at 1 Hz) and n (frequency-dependence coefficient) with lapse time windows from 20 to 50 s in Kumaun Himalaya. Q_0 increases in general with lapse times, whereas the values of n decrease. This is interpreted as the frequency-dependent nature of the attenuation mechanism in the tectonically active Kumaun Himalaya. The reason for different estimates of Q_c for short and longer lapse times can be explained by the different volumes of ellipsoidal region mapped and with decreasing heterogeneity in the crust (Akinici et al., 1995; Ibanez et al., 1990; Roecker et al., 1982). The frequency-dependent coda-wave attenuation (Q_c^{-1}) in Kumaun Himalaya is evident in Figs. 3, 4 and Table 3. Several studies (Aki, 1980; Pulli & Aki, 1981; Roecker et al., 1982) have reported a correlation between n and tectonic activity.

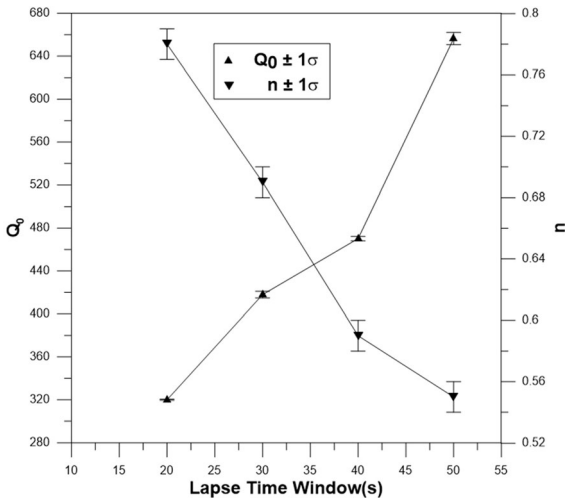


Figure 4

Average values of Q_0 (left side) and n (right side) as functions of lapse time window (LTW). Standard deviations ($\pm 1\sigma$) are shown as error bars

4.2. Seismic Attenuation Model from Body Waves

Table 4 shows the estimated values of the body wave quality factors Q_β , Q_α at six central frequencies (CFs; 1.5, 3, 6, 8, 12 and 18 Hz). The frequency-dependent $Q_\beta(f)$ and $Q_\alpha(f)$ for the entire region are also shown.

For estimation of Q_β , the plots of $\left[\ln \left(\frac{A_\beta(f,r)r^2}{A_c(f,t_c)} \right) \right]$ versus hypocentral distance, r (at $\gamma = 1$), for the different central frequencies were plotted for different events and stations (see Akinci and Eyidogan, 1996; Frankel, 1991) as shown in Fig. 5. Using the

Table 4

Estimated values of the body wave quality factors Q_β , Q_α at the six central frequencies (CFs). The frequency-dependent $Q_\beta(f)$ and $Q_\alpha(f)$ for the entire region are also shown

CF (Hz)	Q_α	Q_β
1.5	54.25	81.24
3	84.02	134.84
6	171.70	252.99
8	218.65	340.71
12	297.73	527.38
18	434.29	846.88
Whole region	$(36.28 \pm 0.05) f^{(0.85 \pm 0.01)}$	$(50.58 \pm 0.15) f^{(0.94 \pm 0.01)}$
$Q_{\alpha, \beta}(f) = Q_0^n$		

ECN method, as described in the previous section, for estimation of Q_α , the plots of $\left[\ln \left(\frac{A_\alpha(f,r)r^2}{A_c(f,t_c)} \right) \right]$ versus hypocentral distance, r , for the different central frequencies were plotted for different events and stations, as shown in Fig. 6. In both Figs. 5 and 6, the regression lines from the least-squares estimate are shown in red color. The values of Q_β and Q_α obtained from slopes of the least-squares fits are shown for each central frequency. The linear least squares regression provides the average values of the quality factor.

4.3. Intrinsic (Q_i^{-1}) and Scattering Attenuation (Q_s^{-1})

The knowledge of the proportionate contributions of intrinsic attenuation (Q_i^{-1}) and scattering attenuation (Q_s^{-1}) to the total attenuation is quite useful to interpret the mechanism of seismic wave energy dissipation. The contributions of scattering and intrinsic attenuation are extracted using Wennerberg's (1993) formulation, using the independent estimates of Q_c (a lapse time of 40 s) and Q_β . The estimated values of Q_i and Q_s at six central frequencies are shown in Table 5. Similarly, Table 6 shows the frequency-dependence relations for Q_s and Q_i . The estimated values of Q_i and Q_s indicate an increase with frequency. As shown in Fig. 7, the relations obtained by using least-squares regression analysis are $Q_i = (231 \pm 0.2) f^{(0.77 \pm 0.01)}$ and $Q_s = (67 \pm 0.5) f^{(0.99 \pm 0.07)}$. This study shows that the intrinsic attenuation (Q_i^{-1}) is less dominant over scattering attenuation (Q_s^{-1}) in the frequency range 1.0–20 Hz. As mentioned earlier, dominant scattering attenuation parameter (Q_s^{-1}) describes the crustal inhomogeneity in the study region due to a multitude of cracks and pores. For comparative analysis of different tectonic regions, such as LH and HH segments, within our study region, we perform comparative analysis as described in subsequent sections below and as depicted in Fig. 8a–d.

To understand the relation between Q_c^{-1} and Q_i^{-1} for the whole region to obtain a broader sense, we observe from Fig. 7 that Q_c^{-1} is close to Q_i^{-1} . These observations are in good agreement with other worldwide studies carried out in tectonic regions (Akinci et al., 1995; Bianco et al., 2002; Frankel &

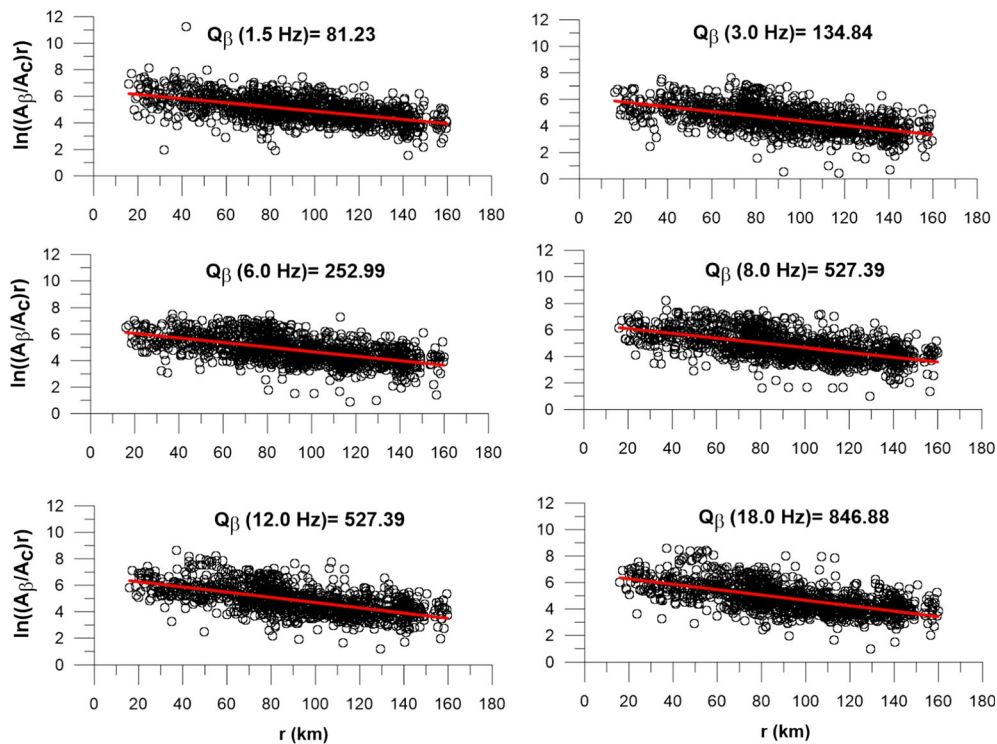


Figure 5

Coda normalized peak amplitude decay of S waves with hypocentral distance at six central frequencies (1.5, 3, 6, 8, 12 and 18 Hz). The regression lines from the least-squares estimate are shown in red color. The values of Q_β obtained from slopes of the least-squares fits are shown for each central frequency

Wennerberg, 1987). In this way, Fig. 9 shows the relation between Q_c^{-1} vs. frequency (Hz) of this study compared to other studies. We provide comparisons with Q_c^{-1} studies, such as Paul et al. (2003) (Kumaun Himalaya); Kumar et al. (2005) (northwest Himalaya, India); Mukhopadhyay et al. (2006) (western Himalaya, India); Sharma et al. (2008) (Kachch, India); Mukhopadhyay et al. (2010) (Garhwal-Kumaun Himalaya); Hazarika et al. (2013) (Sikkim Himalaya, India); Mishra et al. (2020) (northwest Himalaya, India); Padhy et al. (2011) (Andaman, India). Similarly, Figs. 10, 11 and 12 show the essential relations between Q_β^{-1} , Q_α^{-1} with frequency (Hz) and between Q_β and Q_α for this study and compared to other studies. We compare with studies such as Yoshimoto et al. (1993) (in Kanto region, Japan); Chung and Sato (2001) (in southeastern Korea); Sharma et al. (2008) (in Kachch, India); Padhy et al. (2011) (in Bhuj, India); Singh et al. (2012) (in Kumaun Himalaya); Hazarika et al. (2013)

(in Sikkim Himalaya, India); Tripathi et al. (2014) (in Garhwal Himalaya, India); Monika et al. (2020) (in Kumaun Himalaya); Ma and Huang (2020) (in Central and Western Tien Shan); Castro et al. (2021) (in Central Apennines, Italy). We observe that the ratio $Q_\alpha^{-1}/Q_\beta^{-1} > 1$ for the entire frequency range considered. So, in the broader sense, these observations are in agreement with the above studies and with earlier works (such as Canas et al., 1998; Del Pezzo et al., 1995; Giampiccolo et al., 2004; Rautian & Khalturin, 1978). Now, we discuss the observations regarding the two considered tectonic segments in the study region.

5. Observed Patterns Among LH and HH Segments

We provide a more refined perspective of the body wave attenuation characteristics across the LH and HH segments, which has a wider implication for

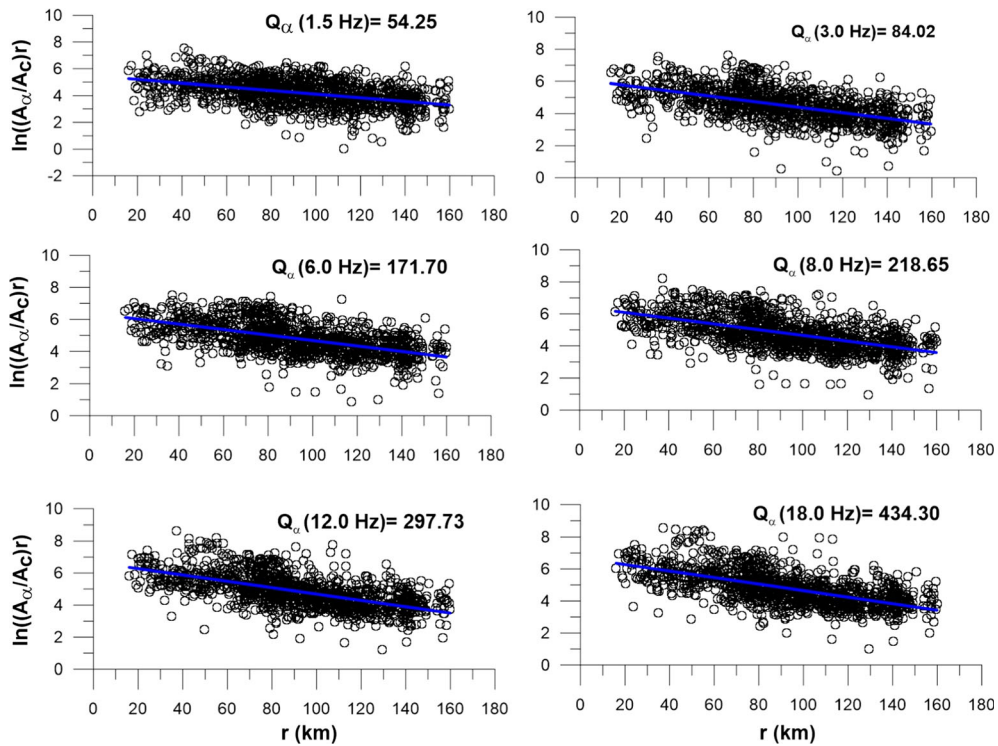


Figure 6

Coda normalized peak amplitude decay of P waves with hypocentral distance at six central frequencies (1.5, 3, 6, 8, 12 and 18 Hz). The regression lines from the least-squares estimate are shown in blue color. The values of Q_α obtained from slopes of the least-squares fits are shown for each central frequency

Table 5

Separation of Q_c (at $LTW = 40$ s) in terms of Q_s and Q_i using Q_β by Wennerberg formulations

CF	Q_c	Q_α	Q_β	Q_s	Q_i	Q_β/Q_α
1.5	442.44	54.25	81.24	114.95	327.52	1.50
3	898.52	84.02	134.84	180.17	535.98	1.61
6	1324.61	171.70	252.99	354.75	881.99	1.47
8	1608.82	218.65	340.71	491.67	1109.70	1.56
12	2170.22	297.73	527.39	796.75	1560.00	1.77
18	3088.33	434.29	846.88	1345.56	2285.08	1.95

LTW lapse time window

Table 6

Frequency-dependence relations for scattering factor, Q_s and intrinsic factor, Q_i

CF	Q_s	Q_i
1.5	114.95	327.52
3	180.17	535.98
6	354.75	881.99
8	491.67	1109.70
12	796.75	1560.00
18	1345.56	2285.08
Whole region	$Q_s = (67 \pm 0.5)f^{(0.99 \pm 0.07)}$	$Q_i = (231 \pm 0.2)f^{(0.77 \pm 0.01)}$

structure and geotechnical analysis. We show the estimations for Q_β , Q_α for the LH and HH segments in Fig. 8a–d and Table 7. We observe that the LH segment has higher values Q_β , Q_α at each of the six frequencies and at 1 Hz (Q_0). The higher values of Q_β , Q_α (implying lower attenuation, Q_β^{-1} , Q_α^{-1}) beneath the crust in the LH segment (as compared to HH segment) might be correlated to the

underthrusting Indian Plate, leading to the fractures, brittle conditions and earthquake ruptures in the crust and uppermost mantle. It is also possible that the diversified geological features and/or varying fluid content in LH may give rise to lower attenuation, Q_β^{-1} , Q_α^{-1} (compared to HH segment). Thus, the LH

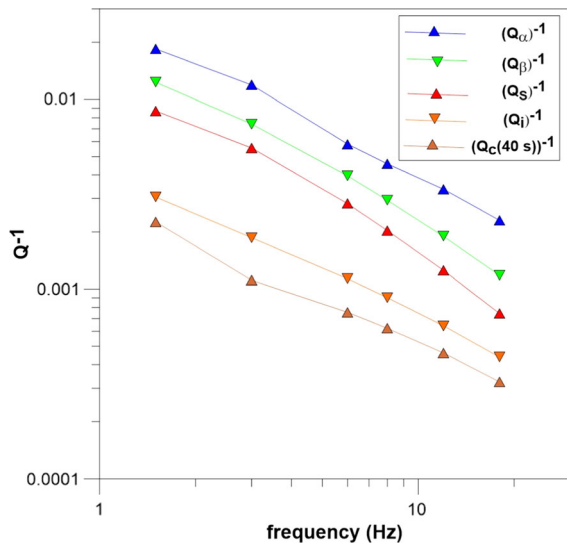


Figure 7

Variation of Q_c^{-1} , Q_β^{-1} , Q_α^{-1} , Q_{sc}^{-1} and Q_i^{-1} with frequency (Hz) for the Kumaun Himalaya in this study

seems to be differentiated from the HH segments in terms of higher extent of fractures and fluids/partial-melts.

6. Geological Implications

In line with the above observations of $Q_\alpha^{-1}/Q_\beta^{-1} > 1$, and the predominance of (Q_s^{-1}) over (Q_i^{-1}) , our investigation seems to indicate the presence of heterogeneities in the form of cracks and pores, possibly related to the multi-scale deformation of the Indian lithosphere. Figure 13 shows the variations of (Q_i^{-1}) , which are compared with other studies, such as, Sharma et al. (2008) (in Kachch, India); Padhy and Subhadra (2013) (in northeast India); Mukhopadhyay et al. (2010) (in Garhwal-Kumaun Himalaya); Hazarika et al. (2013) (in Sikkim Himalaya, India); Del Pezzo et al. (2019) (in Peloritani Mountains, Italy); Akinci et al. (2020) (in Central Apennines, Italy). The variations of (Q_s^{-1}) are shown in Fig. 14, along with comparisons with other studies, as mentioned above. Similarly, Fig. 15 shows the variation of the Q_i^{-1} and Q_s^{-1} in this study, along with comparisons with above-mentioned

studies. Mukhopadhyay et al. (2010) sampled a similar region and have suggested the dominance of scattering attenuation (Q_s^{-1}) over intrinsic attenuation (Q_i^{-1}) . Similar to their results, we also observe that the frequency-dependence parameter 'n' of (Q_s^{-1}) is larger than that of (Q_i^{-1}) , further strengthening the argument and evidence of large-scale heterogeneities. Del-Pezzo et al. (2019) (Peloritani Mountains, Italy) show that scattering attenuation is dominant in the active Peloritani mountains (Italy) below 6 Hz. Similarly, Akinci et al. (2020) indicate similar scattering attenuation (Q_s^{-1}) as obtained in our study region.

On the whole, the substantial frequency dependence of the different attenuation quality factors suggests an essentially heterogeneous crust in the Kumaun Himalaya. The present study shows that $Q_c^{-1} < Q_\beta^{-1}$, but Q_c^{-1} is close to Q_i^{-1} (Fig. 7). The study by Shang and Gao (1988) shows that in a highly heterogeneous and scattering medium, the coda attenuation (Q_c^{-1}) is identical to (Q_i^{-1}) . Our results and observations endorse similar findings.

This study also seems to support Zeng's (1991) radiative transfer theory that Q_i^{-1} and Q_s^{-1} combine in such a way that $Q_c^{-1} < Q_\beta^{-1}$.

Also, the ratio, $(Q_\alpha^{-1}/Q_\beta^{-1}) (> 1$ in our study; as in Fig. 12), indicates a high degree of heterogeneity of the rocks in the crust beneath Kumaun Himalaya. In our study region, the P-wave attenuation seems to be more than S-waves. The ratio, $Q_\alpha^{-1}/Q_\beta^{-1}$, in our study varies between 1.7 and 2.2. Earlier studies like Yoshimoto et al. (1993) and Rautian and Khalturin (1978) found that the ratio, $Q_\alpha^{-1}/Q_\beta^{-1}$, is close to the ratio, V_α/V_β (~ 1.73) (V_α is the P-wave velocity; V_β is the S-wave velocity) value for crustal rocks in their study regions. As per Winkler and Nur (1982) (see Fig. 5 of this reference), $Q_\alpha^{-1}/Q_\beta^{-1}$ ratio is between 1.5 and 2, and V_α/V_β varies between 1.5 and 1.75 for partially saturated ($\sim 90\%$) rocks. A high V_α/V_β ratio possibly indicates a fluid or melt state in rocks as indicated in tomographic studies (Mahesh et al., 2012). The presence and release of fluids cause permeation upwards into the brittle part of the crust, thereby reducing the fault zone friction and leading to

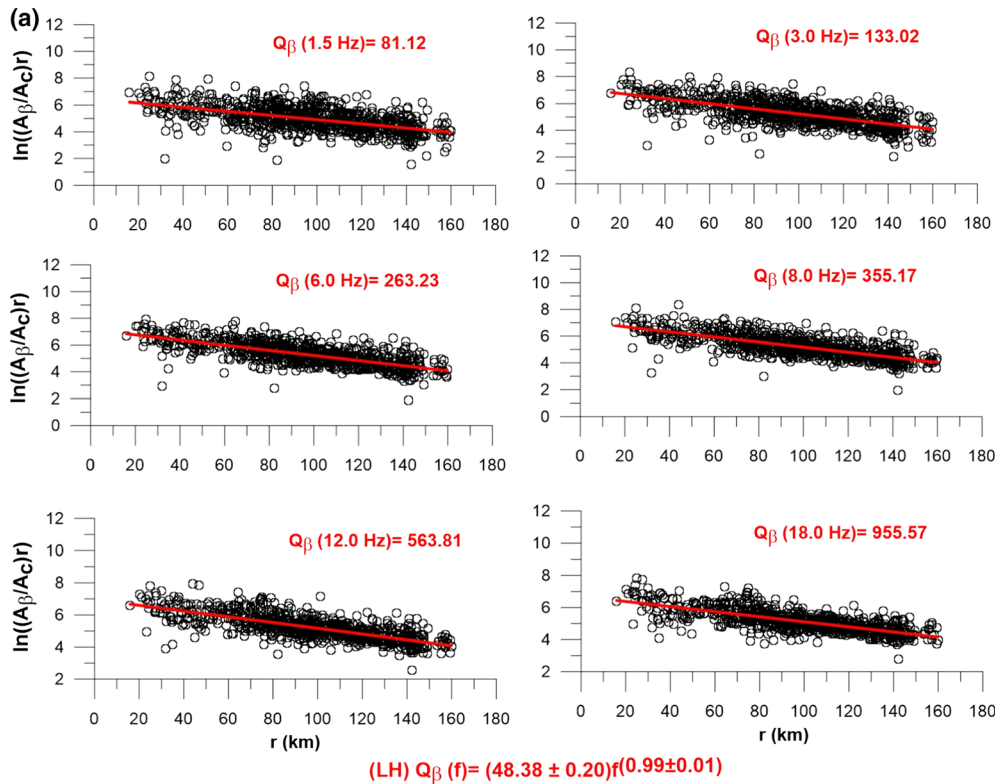


Figure 8

a Coda normalized peak amplitude decay of S waves with hypocentral distance at the six central frequencies for stations in Lower Himalaya (LH) segment. The regression lines from the least-squares estimate are shown in red color. The values of Q_β obtained from slopes of the least-squares fits are shown for each central frequency, and the frequency-dependent power law is shown in red. **b** Coda normalized peak amplitude decay of P waves with hypocentral distance at the six central frequencies for stations in LH segment. The regression lines from the least-squares estimate are shown in blue color. The values of Q_α obtained from slopes of the least-squares fits are shown for each central frequency, and the frequency-dependent power law is shown in blue. **c** Coda normalized peak amplitude decay of S waves with hypocentral distance at the six central frequencies for stations in Higher Himalaya (HH) segment. The regression lines from the least-squares estimate are shown in red color. The values of Q_β obtained from slopes of the least-squares fits are shown for each central frequency, and the frequency-dependent power law is shown in red. **d** Coda normalized peak amplitude decay of P waves with hypocentral distance at the six central frequencies for stations in HH segment. The regression lines from the least-squares estimate are shown in blue color. The values of Q_α obtained from slopes of the least-squares fits are shown for each central frequency, and the frequency-dependent power law is shown in blue

the generation of crustal earthquakes. According to a recent tomography study by the authors (Gupta et al., 2022), the small-, moderate- and strong-magnitude earthquakes are largely restricted to the fluid-trapped portions and quartz-rich rocks in the upper crust, seemingly with a geometrical alignment of the crustal lithology. The studies conducted in similar regions (such as in Mishra et al., 2020; Monika et al. 2020; Singh et al., 2012; Tripathi et al., 2014) and other heterogenous and active regions (such as Kanto

region, Japan, Yoshimoto et al., 1993; Central-East Iran, Mahood et al., 2009; Bhuj region, India, Padhy et al., 2011) indicate a prominent observation of $Q_\alpha^{-1}/Q_\beta^{-1} > 1$. From a perspective of seismic hazard, recent studies in east Asia have investigated the spatial and temporal variations in the crust from shallow earthquakes to understand the cyclic behavior of the occurrence of cracks and their healing (Iqbal et al., 2021). They conclude that the estimates of scattering attenuation (Q_s^{-1}), before and after

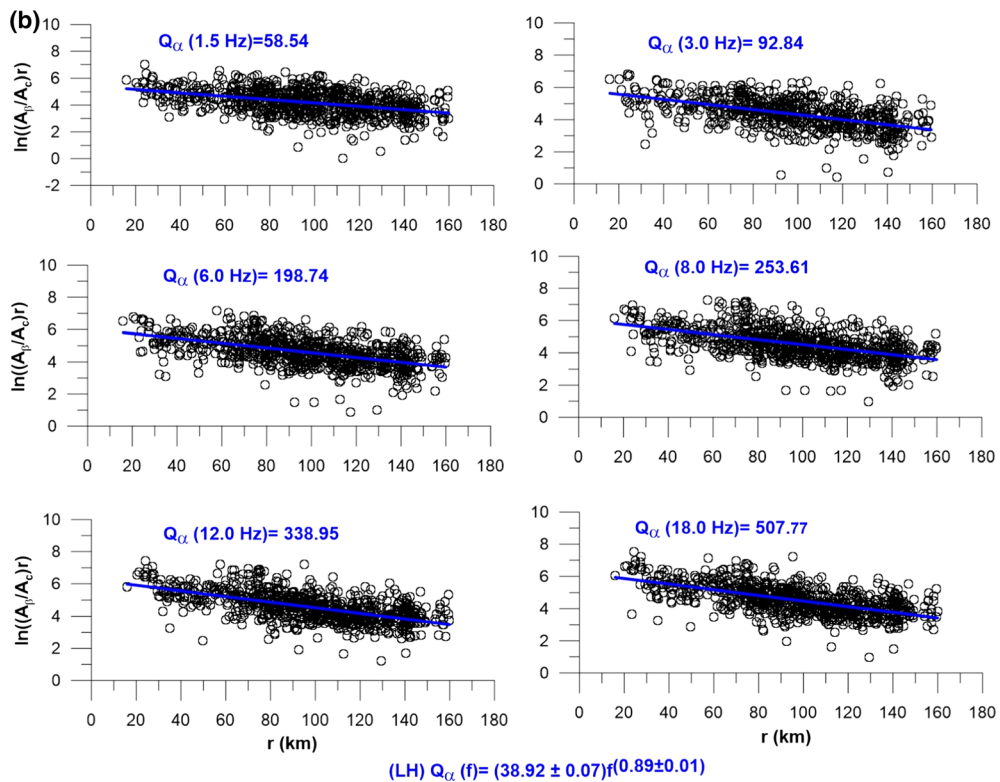


Figure 8
continued

occurrence of events, are powerful means to assess the variations in crustal inhomogeneity due to cracks. Thus, the seismicity in Kumaun Himalaya may enhance the crustal inhomogeneity, thereby presenting a predominantly scattering attenuation model.

In other tectonic domains with intrinsic attenuation (Q_i^{-1}), the role of increased temperature is often suggested in grain boundary sliding beneath the crust, having temperatures > 900 °C. The increased temperature then becomes the primary controlling factor in attenuation (Mitchell, 1995) as the deformation behavior is altered from elastic to anelastic to viscous (Jackson et al., 2002). The hydrothermal reactions cause fluids to rise upward through cracks while allowing them to reside predominantly in the upper crust. Furthermore, the cracks filled with liquids, as

mentioned, affect the attenuation mechanism related to P and S waves. Ashish et al. (2009) have suggested the existence of Miocene leucogranite plutons, a magmatic byproduct resulting from the Indo-Asian collision.

In general, our results provide a first-order characterization of the nature of the crustal rocks and seismic attenuation and are seen to match well with other active regions. Our results show that the LH and HH segments are well differentiated in terms of rock lithology and the scattering attenuation is the dominant mechanism of seismic attenuation in the whole study region. We note that model assumptions might result in simplification of a complex structure, as observed by various researchers. We believe that this study of seismic attenuation in such a complex region

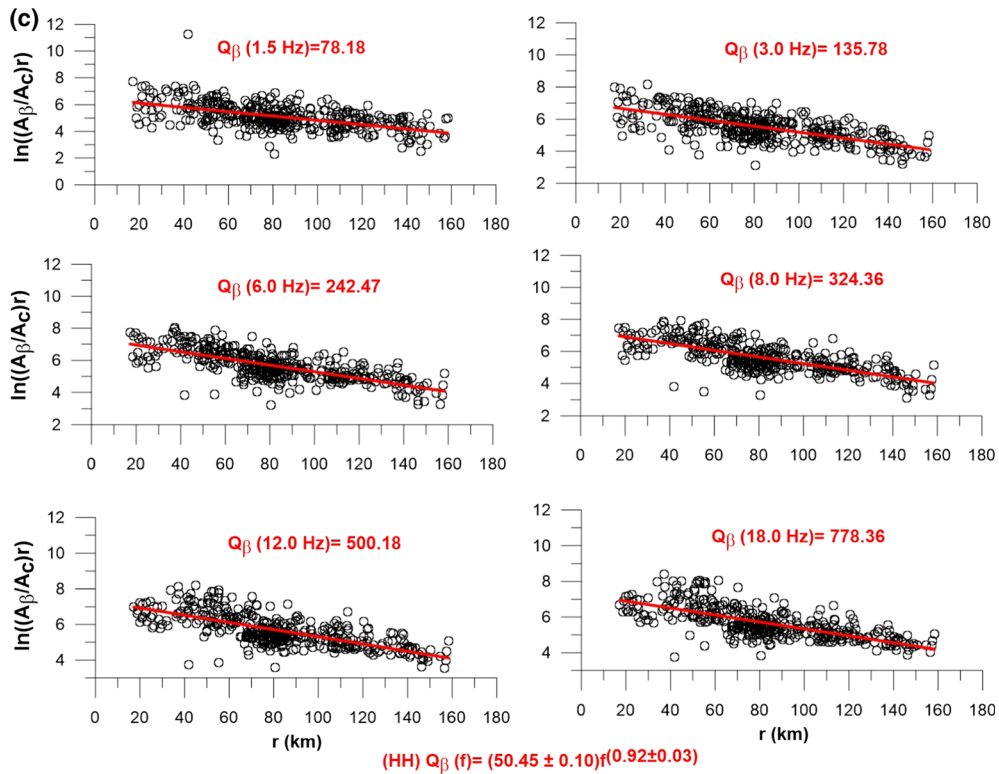


Figure 8
continued

can add information which are playing a fundamental role in active tectonic settings. A comparative analysis of different modeling techniques may bring out deeper insights, which may be explored in future studies.

7. Conclusions

Seismic wave attenuation in the Kumaun Himalaya has been estimated using body and coda waves at 1–20 Hz using about 300 local events. Seismic attenuation is analyzed for the entire study region and distinct tectonic belts such as the Lesser Himalaya (LH) and the Higher Himalaya (HH) segments. Coda wave attenuation (Q_c^{-1}) and body wave attenuation

$[Q_{\alpha}^{-1}$ (P-wave), Q_{β}^{-1} (S-wave)] were estimated using single isotropic-scattering model and extended coda-normalization method, respectively. The estimated attenuation mechanisms show a strong dependence on frequency, expressed as power laws ($Q_c = Q_0 f^n$). From our Q_c analysis, Q_0 and n vary as 320 and 0.78 for lapse time window 20 s to 656 and 0.55 at lapse time window 50 s. The body waves Q are expressed as $Q_{\alpha} = (36.28 \pm 0.05)f^{(0.85 \pm 0.01)}$ and $Q_{\beta} = (50.58 \pm 0.15)f^{(0.94 \pm 0.01)}$. We observe that the ratio $Q_{\alpha}^{-1}/Q_{\beta}^{-1}$ is larger than unity for the whole frequency range, which is interpreted as the effect of seismically active regions and heterogeneous crustal regimes. The heterogeneities, however, may be varied and the result of fractures and the presence of pore fluids or partial melts in the upper crust.

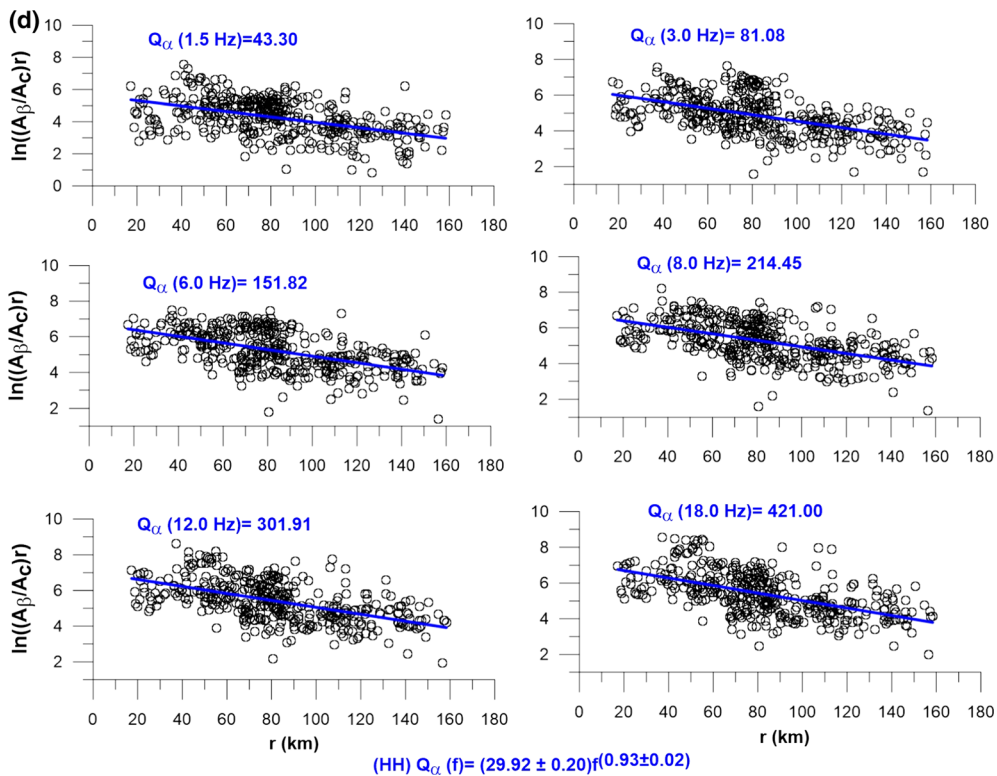


Figure 8 continued

Additionally, we show that the Lesser Himalaya (LH) and the Higher Himalaya (HH) segments are characterized by differentiated rock lithology, with possible roles of underthrusting and deformation. Apart from that, the extracted intrinsic absorption (Q_i^{-1}) and scattering (Q_s^{-1}) attenuation indicate the dominance of scattering attenuation (Q_s^{-1}). The results also show that (1) Q_c^{-1} is less than Q_{β}^{-1} ; (2)

the ratio ($Q_{\alpha}^{-1}/Q_{\beta}^{-1}$) lies between 1.7 and 2.25, indicating the presence of partially saturated rocks in the crust beneath Kumaun Himalaya. The LH and HH tectonic segments imply divergent geology, indicate varying attenuative characteristics, and have a significant role in seismic hazard analysis in Kumaun Himalaya.

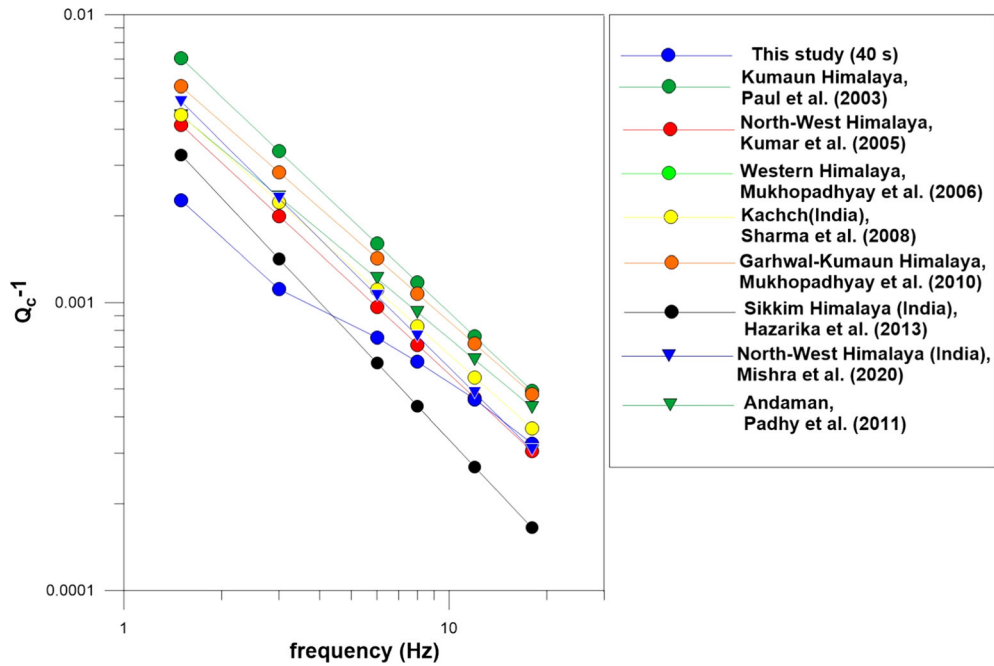


Figure 9
Comparison of Q_c^{-1} with frequency (Hz) of our study with other studies

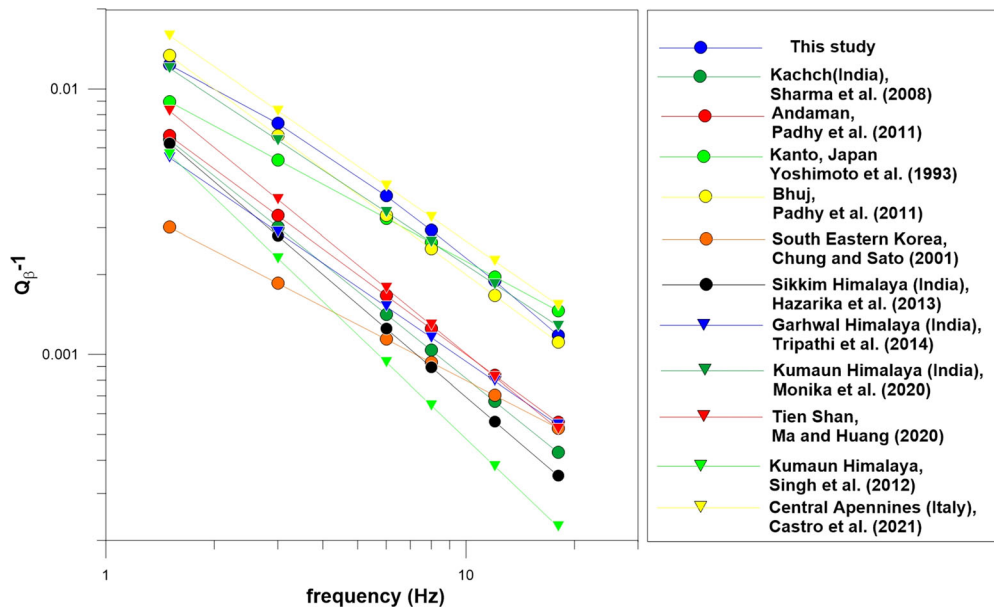


Figure 10
Comparison of Q_β^{-1} of our study with other studies in India and other parts of the world

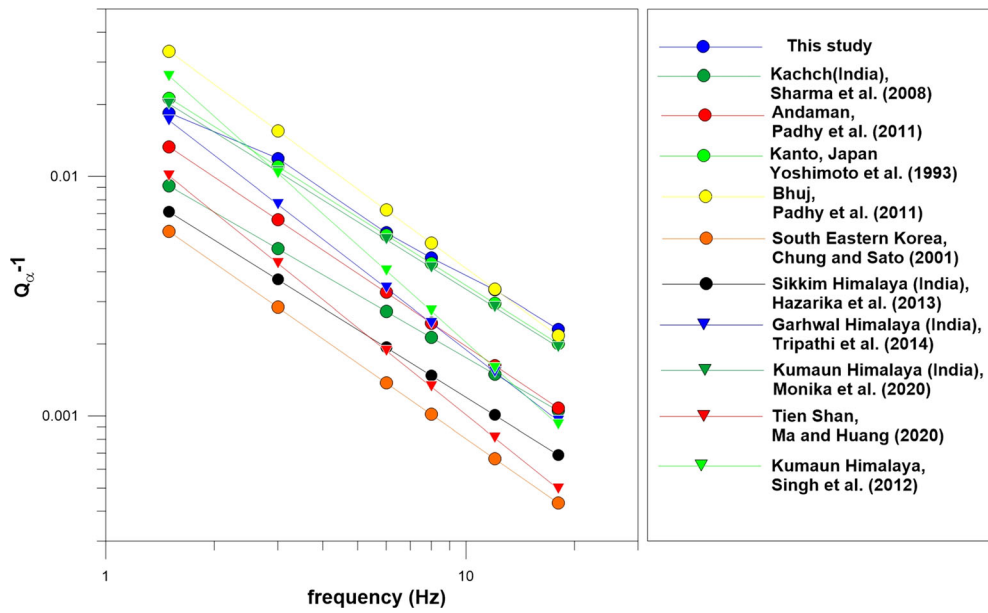


Figure 11

Comparison of Q_{α}^{-1} with frequency (Hz) of our study with other studies in India and other parts of the world

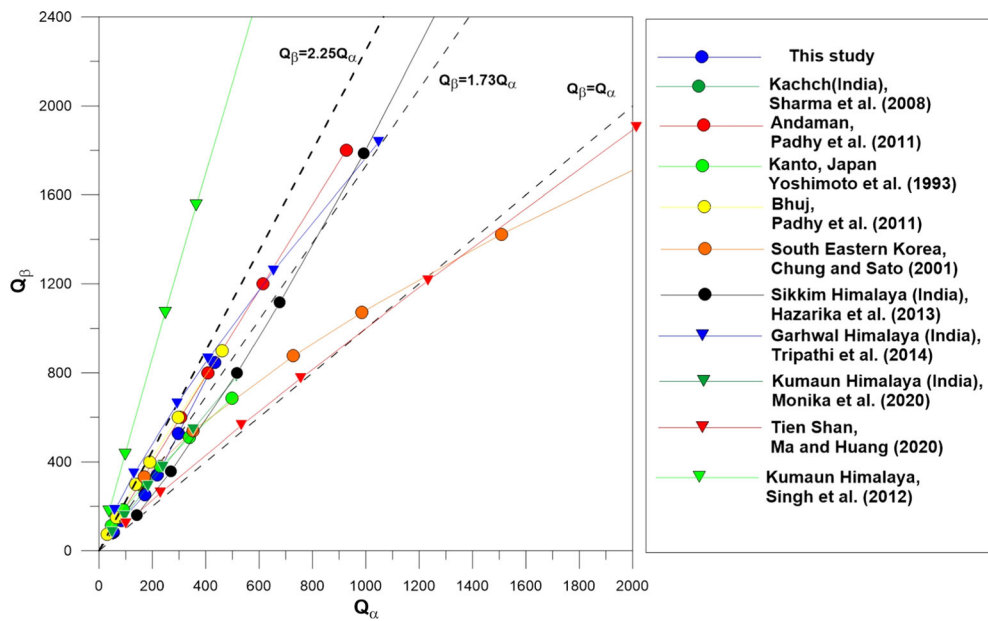


Figure 12

Comparison of variation of Q_{β} , Q_{α} and evaluation of the $\left(\frac{Q_{\beta}}{Q_{\alpha}}\right)$ ratio obtained in this study and as reported by other studies in India and other parts of the world

Table 7

Estimated values of the body wave quality factors Q_β , Q_α at six central frequencies (CFs) and frequency-dependent $Q_\beta(f)$, $Q_\alpha(f)$ for the LH and HH segments

CF (Hz)	Lesser Himalaya (LH)		Higher Himalaya (HH)	
	Q_α	Q_β	Q_α	Q_β
1.5	58.54	81.12	43.30	78.18
3	92.84	133.02	81.08	135.78
6	198.74	263.27	159.82	242.47
8	253.62	355.17	214.45	324.36
12	338.95	563.81	301.91	500.18
18	507.77	955.57	420.16	778.36
$Q_{\alpha, \beta}(f) = Q_0 f^n$	$(38.92 \pm 0.07)f^{(0.89 \pm 0.02)}$	$(48.38 \pm 0.22)f^{(0.99 \pm 0.01)}$	$(29.92 \pm 0.01)f^{(0.93 \pm 0.02)}$	$(50.45 \pm 0.10)f^{(0.92 \pm 0.01)}$

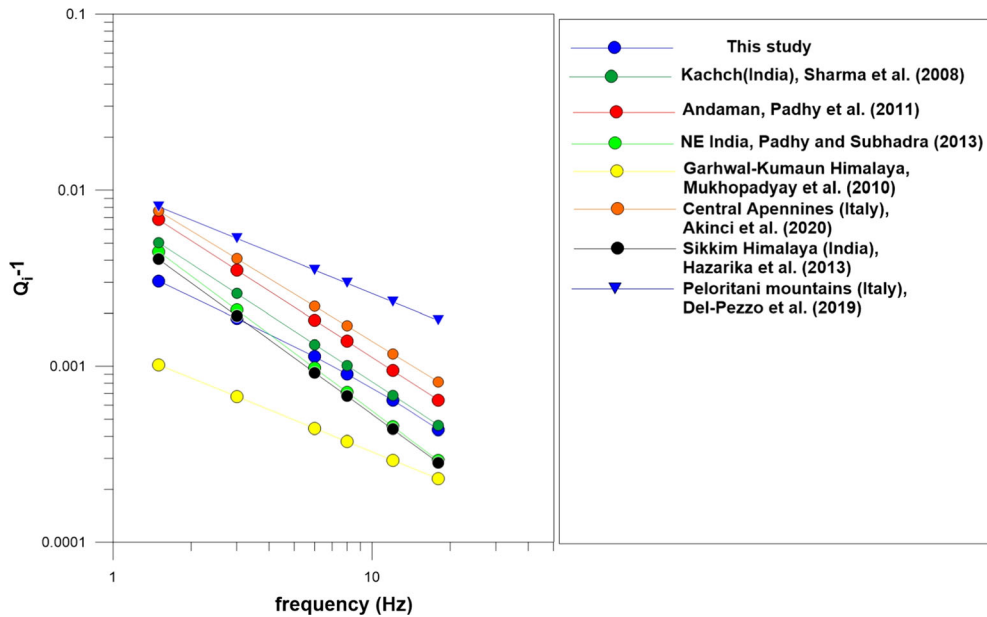


Figure 13

Comparison of Q_i^{-1} with frequency (Hz) of this study and other studies in India and other parts of the world

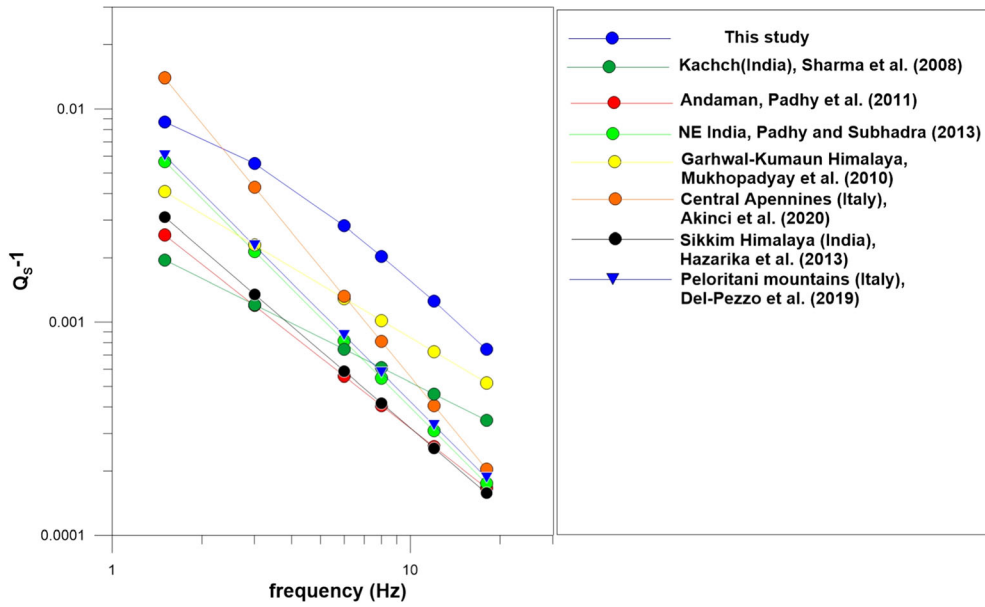


Figure 14

Comparison of Q_s^{-1} with frequency (Hz) of this study and other studies in India and other parts of the world

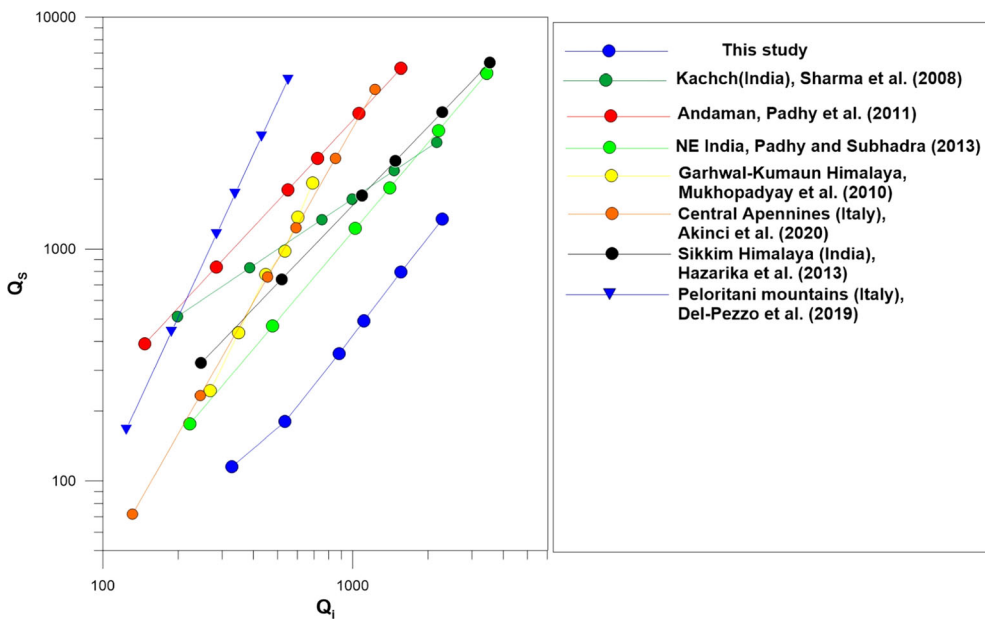


Figure 15

Comparison of Q_i and Q_s in this study with other studies in India and other parts of the world

Acknowledgements

The authors thank CSIR-NGRI for granting permission to publish this work. Author (SK) gratefully acknowledges the early guidance of Dr. Dinesh Kumar in the computation of seismic attenuation. All the field members of the seismological field in Kumaun-Garhwal Himalaya are duly acknowledged for their hard work and data acquisition. We acknowledge the support under CSIR-NGRI projects SHIVA [MLP0001-28-FBR-1] and ProbHim [MLP-FBR-003]. The authors sincerely acknowledge the Editor, Dr Yangfan Deng, and the three anonymous reviewers whose suggestions have significantly improved the manuscript. The CSIR-NGRI reference number of the manuscript is NGRI/Lib/2022/ Pub-09.

Author Contributions KS: Conceptualization, data curation, visualization, methodology, writing—original draft preparation, reviewing and editing. SG: Visualization, writing—reviewing and editing.

Funding

CSIR NGRI.

Availability of Data and Material

Data are available upon request to the Director, CSIR-NGRI.

Declarations

Conflicts of interest The authors declare no competing interests.

Publisher's Note Springer Nature remains neutral with regard to jurisdictional claims in published maps and institutional affiliations.

REFERENCES

- Aki, K. (1969). Analysis of the seismic coda of local earthquakes as scattered waves. *Journal of Geophysical Research*, 74(2), 615–631.
- Aki, K. (1980). Scattering and attenuation of shear waves in lithosphere. *Journal of Geophysical Research*, 85, 6496–6504.
- Aki, K., & Chouet, B. (1975). Origin of coda waves; source, attenuation and scattering effects. *Journal of Geophysical Research*, 80, 3322–3342.
- Akinci, A., Del Pezzo, E., & Ibanez, J. M. (1995). Separation of scattering and intrinsic attenuation in southern Spain and western Anatolia (Turkey). *Geophysical Journal International*, 121, 337–353.
- Akinci, A., Del Pezzo, E., & Malagnini, L. (2020). Intrinsic and scattering seismic wave attenuation in the Central Apennines (Italy). *Physics of the Earth and Planetary Interiors*, 303, 106498. <https://doi.org/10.1016/j.pepi.2020.106498>
- Akinci, A., & Eyidogan, H. (1996). Frequency-dependent attenuation of S and coda waves in Erzincan region (Turkey). *Physics of the Earth and Planetary Interiors*, 97, 109–119.
- Ashish, P. A., Rai, S. S., & Gupta, S. (2009). Seismological evidence for shallow crustal melt beneath the Garhwal High Himalaya, India: Implications for Himalayan channel flow. *Geophysical Journal International*, 177(1), 1111–1120.
- Bianco, F., Del Pezzo, E., Castellano, M., Ibanez, J., & Di Luccio, F. (2002). Separation of intrinsic and scattering seismic attenuation in the Southern Apennine zone, Italy. *Geophysics Journal International*, 150, 10–22.
- Bilham, R., Larson, K., & Freymueller, J. (1997). GPS measurements of present day convergence across the Nepal Himalaya. *Nature*, 386, 61–64.
- Burchfiel, C., Zhiliang, C., Hodges, K. V., Yuping, L., Royden, L., Changrong, D., & Jiene, X. (1992). The south Tibetan detachment system, Himalayan orogen: Extension contemporaneous with and parallel to shortening in a collisional mountain belt. *Special Paper Geology Society of America*, 269, 41.
- Burg, J. P., & Chen, G. M. (1984). Tectonics and structural zonation of southern Tibet. *Nature*, 311, 219–223.
- Canas, J. A., Ugalde, A., Pujades, L. G., Carracedo, J. C., Soler, V., & Blanco, M. J. (1998). Intrinsic and scattering seismic wave attenuation in the Canary Islands. *Journal of Geophysical Research*, 103(15037–15), 050.
- Castro, R. R., Pacor, F., & Spallarossa, D. (2021). Depth-dependent shear-wave attenuation in central Apennines, Italy. *Pure Applied Geophysics*, 178, 2059–2075. <https://doi.org/10.1007/s00024-021-02744-9>
- Chung, T. W., & Sato, H. (2001). Attenuation of high frequency P and S waves in the crust of southeastern South Korea. *Bulletin of the Seismological Society of America*, 91, 1867–1874.
- Dainty, A. M. (1981). A scattering model to explain seismic Q observations in the lithosphere between 1 and 30 Hz. *Geophysical Research Letters*, 8, 1126–1128.
- Del Pezzo, E., Giampiccolo, E., Tuvé, T., Di Grazia, G., Gresta, S., & Ibàñez, J. M. (2019). Study of the regional pattern of intrinsic and scattering seismic attenuation in Eastern Sicily (Italy) from local earthquakes. *Geophysical Journal International*, 218(2), 1456–1468. <https://doi.org/10.1093/gji/ggz208>
- Del Pezzo, E., Ibanez, J., Morales, J., Akinci, A., & Maresca, R. (1995). Measurements of intrinsic and scattering seismic attenuation in the crust. *Bull Seismology Society of America*, 85, 1373–1380.
- Fehler, M., Hoshihara, M., Sato, H., & Obara, K. (1992). Separation of scattering and intrinsic attenuation for the Kanto-Tokai region, Japan, using measurements of S-wave energy vs hypocentral distance. *Geophysics Journal International*, 108, 787–800.
- Frankel, A. (1991). Mechanisms of Seismic Attenuation in the Crust: Scattering and anelasticity in New York State, South

- Africa, and Southern California. *Journal of Geophysics Research*, 96, 6269–6289.
- Frankel, A., McGarr, A., Bicknell, J., Mori, J., Seeber, L., & Cranswick, E. (1990). Attenuation of high-frequency shear waves in the crust: Measurements from New York State, South Africa, and Southern California. *Journal of Geophysical Research*, 95, 17441–17457.
- Frankel, A., & Wennerberg, L. (1987). Energy flux model of seismic coda: Separation of scattering and intrinsic attenuation. *Bulletin Seismology Society of America*, 77, 1223–1251.
- Gao, L. S., Lee, L. C., Biswas, N. N., & Aki, K. (1983). Comparison of the effects between single and multiple scattering on coda waves for local earthquakes. *Bulletin of the Seismological Society of America*, 73, 377–389.
- Giampiccolo, E., Gresta, S., & Rasconà, F. (2004). Intrinsic and scattering attenuation from observed seismic codas in south-eastern Sicily (Italy). *Physics Earth Planet International*, 145, 55–66.
- Giampiccolo, E., Tusa, G., Langer, H., & Gresta, S. (2002). Attenuation in southeastern Sicily (Italy) by applying different coda methods. *Journal of Seismology*, 6, 487–501.
- Gupta, S., Mahesh, P., Nagaraju, K., Sivaram, K., & Paul, A. (2022). 3-D seismic velocity structure of the Kumaun-Garhwal (Central) Himalaya: Insight into the Main Himalayan Thrust and earthquake occurrence. *Geophysical Journal International*, 229(1), 138–149. <https://doi.org/10.1093/gji/ggab449>
- Gusev, A. A., & Abubakirov, I. R. (1987). Monte-Carlo simulation of record envelope of a near earthquake. *Physics of the Earth and Planetary Interiors*, 49, 30–36.
- Hazarika, P., Kumar, M. R., & Kumar, D. (2013). Attenuation character of seismic waves in Sikkim Himalaya. *Geophysical Journal International*, 195, 544–557.
- Ibanez, J. M., Del Pezzo, E., De Miguel, F., Herraiz, M., Alguacil, G., & Morales, J. (1990). Depth dependent seismic attenuation in the Granada zone (southern Spain). *Bulletin of the Seismological Society of America*, 80, 1232–1244.
- Iqbal, M. Z., Chung, T. W., Nam, M. J., & Yoshimoto, K. (2021). Temporal variation in scattering and intrinsic attenuation due to earthquakes in East Asia. *Science and Reports*, 11, 11260. <https://doi.org/10.1038/s41598-021-90781-8>
- Jackson, I., Fitzgerald, J. D., Faul, U. H., & Tan, B. H. (2002). Grain-size-sensitive seismic wave attenuation in polycrystalline olivine. *Journal of Geophysics Research*, 107, ECV5.
- Jin, A., & Aki, K. (1989). Spatial and temporal correlation between coda Q^{-1} and seismicity and its physical mechanism. *Journal of Geophysics Research*, 94, 14041–14059.
- Knopoff, L. (1964). *Q. Rev Geophysics*, 2, 625–660.
- Kumar, N., Parvez, I. A., & Virk, H. S. (2005). Estimation of coda wave attenuation for NW Himalayan region using local earthquakes. *Physics of the Earth and Planetary Interiors*, 151, 243–258. <https://doi.org/10.1016/j.pepi.2005.03.010>
- Larson, K. M., Burgmann, R., & Bilham, R. (1999). Freymueller JT (1999) Kinematics of the India-Eurasia collision zone from GPS measurements. *Journal of Geophysical Research*, 104, 1077–1093.
- Le Fort, P. (1996). Evolution of the Himalaya. In A. Yin & M. Harrison (Eds.), *The tectonic evolution of Asia* (pp. 95–109). Press.
- Le Fort, P., Cuney, M., Deniel, C., France-Lanord, C., Sheppard, S. M. F., Upreti, B. N., & Vidal, P. (1987). Crustal generation of the Himalayan leucogranites. *Tectonophysics*, 134, 39–57.
- Ma, X., & Huang, Z. (2020). Attenuation of high-frequency P and S waves in the crust of Central and Western Tien Shan. *Pure Applied Geophysics*, 177, 4127–4142. <https://doi.org/10.1007/s00024-020-02504-11>
- Mahesh, P., Gupta, S., Rai, S. S., & Sarma, P. R. (2012). Fluid driven earthquakes in the Chamoli Region, Garhwal Himalaya: Evidence from local earthquake tomography. *Geophysical Journal International*, 191, 1295–1304.
- Mahesh, P., Rai, S. S., Sivaram, K., Paul, A., Gupta, S., Sarma, P. R., & Gaur, V. K. (2013). One dimensional reference velocity model and precise locations of earthquake hypocenters in the Kumaon-Garhwal Himalaya. *Bulletin Seismology Society of America*, 103, 328–339.
- Mahood, M., Hamzehloo, H., & Doloei, G. J. (2009). Attenuation of high frequency P and S waves in the crust of the East-Central Iran. *Geophysical Journal International*, 179, 1669–1678.
- Matsumoto, S., & Hasegawa, A. (1989). Two-dimensional coda Q structure beneath Tohoku, NE Japan. *Geophysics Journal International*, 99, 101–108.
- Mayed, K., Koyanagi, S., Hoshiya, M., Aki, K., & Zeng, Y. (1992). A comparative study of scattering, intrinsic and coda Q^{-1} for Hawaii, Long Valley, and Central California between 1.5 and 15 Hz. *Journal of Geophysical Research*, 97, 6661–6674.
- Mishra, O. P., Vandana, V. K., & Gera, S. K. (2020). A new insight into seismic attenuation characteristics of Northwest Himalaya and its surrounding region: Implications to structural heterogeneities and earthquake hazards. *Physics of the Earth and Planetary Interiors*, 306(106500), 0031–9201. <https://doi.org/10.1016/j.pepi.2020.106500>
- Mitchell, B. J. (1981). Regional variation and frequency dependence of Q in the crust of the United States. *Bulletin of the Seismological Society of America*, 71, 1531–1538.
- Mitchell, B. J. (1995). Anelastic structure and evolution of the continental crust and upper mantle from seismic surface wave attenuation. *Revision Geophysics*, 33(4), 441–462.
- Molnar, P., England, P., & Martinod, J. (1993). Mantle dynamics, the uplift of the Tibetan Plateau, and the Indian monsoon. *Reviews of Geophysics*, 31, 357–396.
- Monika., Kumar, P., Sandeep., Kumar, S., Joshi, A., & Devi, S. (2020). Spatial variability studies of attenuation characteristics of $Q\alpha$ and $Q\beta$ in Kumaon and Garhwal region of NW Himalaya. *Natural Hazards*, 103, 1219–1237. <https://doi.org/10.1007/s11069-020-04031-7>
- Mukhopadhyay, S., & Sharma, J. (2010). Attenuation characteristics of Garhwal-Kumaun Himalayas from analysis of coda of local earthquakes. *Journal of Seismology*, 14(4), 693–713.
- Mukhopadhyay, S., Sharma, J., Del-Pezzo, E., & Kumar, N. (2010). Study of attenuation mechanism for Garhwal-Kumaun Himalayas from analysis of coda of local earthquakes. *Physics of the Earth and Planetary Interiors*, 180, 7–15.
- Mukhopadhyay, S., Tyagi, C., & Rai, S. S. (2006). The Attenuation mechanism of seismic waves in northwestern Himalayas. *Geophysical Journal International*, 167, 354–360.
- Ni, J., & Barazangi, M. (1984). Seismotectonics of the Himalayan collision zone: Geometry of the underthrusting Indian plate beneath the Himalayas. *Journal of Geophysical Research*, 89, 1147–1163.
- Padhy, S., & Subhadra, N. (2013). Separation of intrinsic and scattering seismic wave attenuation in Northeast India. *Geophysical Journal International*, 195, 1892–1903.

- Padhy, S., Subhadra, N., & Kayal, J. R. (2011). Frequency-dependent attenuation of body and coda waves in the Andaman Sea basin. *Bulletin of the Seismological Society of America*, 101(1), 109–125. <https://doi.org/10.1785/0120100032>
- Patane, D., Ferrucci, F., & Gresta, S. (1994). Spectral features of microearthquakes in volcanic areas: attenuation in the crust and amplitude response of the site at Mt. Etna, Italy. *Bulletin Seismology Society of America*, 84, 1842–1860.
- Paul, A., Gupta, S. C., & Pant, C. (2003). Coda Q estimates for Kumaun Himalaya. *Proceedings Indian Academy Science (earth Planetary Science)*, 112, 569–576.
- Pulli, J. J. (1984). Attenuation of coda waves in New England. *Bulletin of the Seismological Society of America*, 74, 1149–1166.
- Pulli, J. J., & Aki, K. (1981). Attenuation of seismic waves in the lithosphere: Comparison of active and stable areas. In J. E. Beavers (Ed.), *Earthquakes and Earthquake Engineering: The Eastern US* (pp. 129–141). Ann Arbor Science Publishers.
- Rautian, T. G., & Khalturin, V. I. (1978). The use of coda for determination of the earthquake source spectrum. *Bulletin of the Seismological Society of America*, 68, 923–948.
- Roecker, S. W., Tucker, B., King, J., & Hartzfield, D. (1982). Estimates of Q in Central Asia as a function of frequency and depth using the coda of locally recorded earthquakes. *Bulletin of the Seismological Society of America*, 72, 129–149.
- Sato, H. (1978). Mean free path of S-waves under the Kanto district of Japan. *Journal of Physics of the Earth*, 26(2), 185–198.
- Sato, H. (1982). Attenuation of S-waves in the lithosphere due to scattering by its random velocity structure. *Journal of Physics of the Earth*, 87, 7779–7785.
- Sato, H., & Fehler, M. (1998). *Seismic wave propagation and scattering in the heterogeneous earth* (Vol. 308, p. 319). Springer.
- Searle MP (1991) *Geology and Tectonics of the Karakoram Mountains*. John Wiley & Sons, Chichester, with Geological Map of the Central Karakoram, scale 1:250,000. Department Earth Sciences, University of Oxford, Oxford.
- Seeber L, Armbruster J (1981) Great detachment earthquakes along the Himalayan arc and long-term forecasting I Earthquake Prediction. An International Review D.W Simpson, P.G. Richards (Eds.), Am Geophys Union. Maurice Ewing Ser., 4:254–279
- Shang, T., & Gao, L. (1988). Transportation theory of multiple scattering and its application to seismic coda waves of impulse source. *Sci Sinica Ser. B*, 31, 1503–1514.
- Sharma, B., Gupta, A. K., Kameswari Devi, D., Kumar, D., Teotia, S. S., & Rastogi, B. K. (2008). Attenuation of high-frequency seismic waves in Kachchh Region, Gujarat, India. *Bulletin of the Seismological Society of America*, 98(5), 2325–2340. <https://doi.org/10.1785/0120070224>
- Sheehan, A. F., de la Torre, T. L., Monsalve, G., Abers, G. A., & Hacker, B. R. (2014). Physical state of himalayan crust and uppermost mantle: Constraints from seismic attenuation and velocity tomography. *J Geophys Res: Solid Earth*, 119(1), 567–580. <https://doi.org/10.1002/2013JB010601>
- Singh, C., Bharathi, V. S., & Chadha, R. (2012). Lapse time and frequency-dependent attenuation characteristics of Kumaun Himalaya. *Journal of Asian Earth Sciences*, 54, 64–71.
- Singh, S., & Herrmann, R. B. (1983). Regionalization of crustal coda Q in the continental United States. *J Geophys Res Solid Earth*, 88(B1), 527–538.
- Tapponnier P, Peltzer G, Armijo R (1986) On the mechanics of the collision between India and Asia, in Collision Tectonics, Geological Society of London Special Publication, pp. 115–157, eds Coward M.P. Ries A.C.
- Tripathi, J. N., Singh, P., & Sharma, M. (2014). Attenuation of high-frequency P- and S-waves in Garhwal Himalaya, India. *Tectonophysics*, 636, 216–227. <https://doi.org/10.1016/j.tecto.2014.08.015>
- Vassiliou M, Salvado CA, Tittman BR (1982) Seismic attenuation, in CRC Handbook of Physical Properties of Rocks, R. S. Carmichael (Editor), 3, CRC Press, Boca Raton, Florida
- Wennerberg, L. (1993). Multiple-scattering interpretations of coda-Q measurements. *Bulletin of the Seismological Society of America*, 83, 279–290.
- Winkler, K. W., & Nur, A. (1982). Seismic attenuation: Effects of pore fluids and frictional sliding. *Geophysics*, 47, 1–15.
- Yoshimoto, K. H., Sato, H., & Ohtake, M. (1993). Frequency dependent attenuation of P and S waves in the Kanto area, Japan. Based on the Coda Normalization Method. *Geophysics Journal International*, 114, 165–174.
- Zeng, Y., Su, F., & Aki, K. (1991). Scattered wave energy propagation in a random isotropic scattering medium, I, theory. *Journal of Geophysical Research*, 96, 607–619.